Supporting Information

Oxygen Atom Transfer and Oxidative Water Incorporation in Cuboidal Mn_3MO_n Complexes based on Synthetic, Isotopic Labeling, and Computational Studies

Jacob S. Kanady[1], Jose L. Mendoza-Cortes[1], Emily Y. Tsui, Robert J. Nielsen, William A. Goddard III*, Theodor Agapie*

Department of Chemistry and Chemical Engineering and Materials and Process Simulation Center, California Institute of Technology, 1200 E. California Blvd MC 127-72, Pasadena CA, USA. [1]These authors contributed equally.

E-mail: wag@wag.caltech.edu, agapie@caltech.edu

Contents

List of Figures

List of Tables

Part I

Theory/Computation

1 Computational methodology

Quantum Mechanical calculations were carried out using the B3LYP hybrid functional [1,2] as implemented in the Jaguar code. [3] For optimizing the structures we used the 6-31G** basis set for C, H, N, P, and O and LACVP** basis set and effective core potential for Mn and Ca. [4] All geometries were optimized using the analytic Hessian to determine that the local minima have no negative curvatures (no imaginary frequencies) and that each transition state (TS) has one and only one negative eigenvalue. We then carried out single point energy calculations using the extended basis set: 6-311G**++ for C, H, N, P, and O (to which an additional *d*-funtion with exponent $\alpha = 1.35$ was added to phosphorus [5]), LACV3P**++ for Mn (to which two *f*-funtion with exponents $\alpha = 0.795$ and $\alpha = 3.118$ were added to Manganese [5]); and LAV3D** for Ca to obtain the final energetics. [4]. We included solvation effects using the Poisson-Boltzmann continuum (PBF) approximation [6] for dimethylformamide (DMF; ϵ=36.7 and r_0=2.49), dimethylacetamide (DMA; ϵ=38.85 and r_0=2.64), and acetonitrile (AN; ϵ=37.5 and r_0=2.18).

Free energies used in the calculation of oxidation potentials are:

$$G_{298\ \mathrm{K}} = E_{\mathrm{elec}} + G_{\mathrm{solv}} + \mathrm{ZPE} + H_{\mathrm{vib}} + \frac{n}{2}kT - TS_{\mathrm{vib}} \tag{1}$$

where consider electronic (elec), solvation (solv), vibrational (vib), and zero point vibrational energy (ZPE). $n = 12$ accounts for the potential and kinetic energies of the translational and rotational modes.

Energies discussed in the text include solvation and zero point vibrational energies:

$$E_{0\ \mathrm{K}} = E_{\mathrm{elec}} + G_{\mathrm{solv}} + \mathrm{ZPE} \tag{2}$$

1.1 Validation of the Computational Methodology: Geometry (*continuation*)

In **Figure 4** we showed the validation of our methodology to predict and reproduce the properties of compounds **2** and **4**, where we compared the X-ray diffraction (XRD) coordinates with the minimized structures obtained from QM calculations.

However, we need to interrogate many properties of these compounds such as electronic states, geometry optimization for derivatives and having to do this for 147 or 134 atoms is too expensive computationally. We postulate that the $\mathbf{H_3L}$ ligand, while serving to support the metallic cluster, should not participate in the important electrochemical reactions. Thus we simplified our compound by removing the four benzene rings at the bottom and the three unbound pyridines. In addition we fix the carbon that bridges the oxo and bound pyridine in order to mimic the presence of the stiffness of the full $\mathbf{H_3L}$ ligand. The results are shown in Figure S1. We use these model compounds for initial interrogation of properties and then we put back the entire ligand to make the final calculation of properties for **2** and **4**.

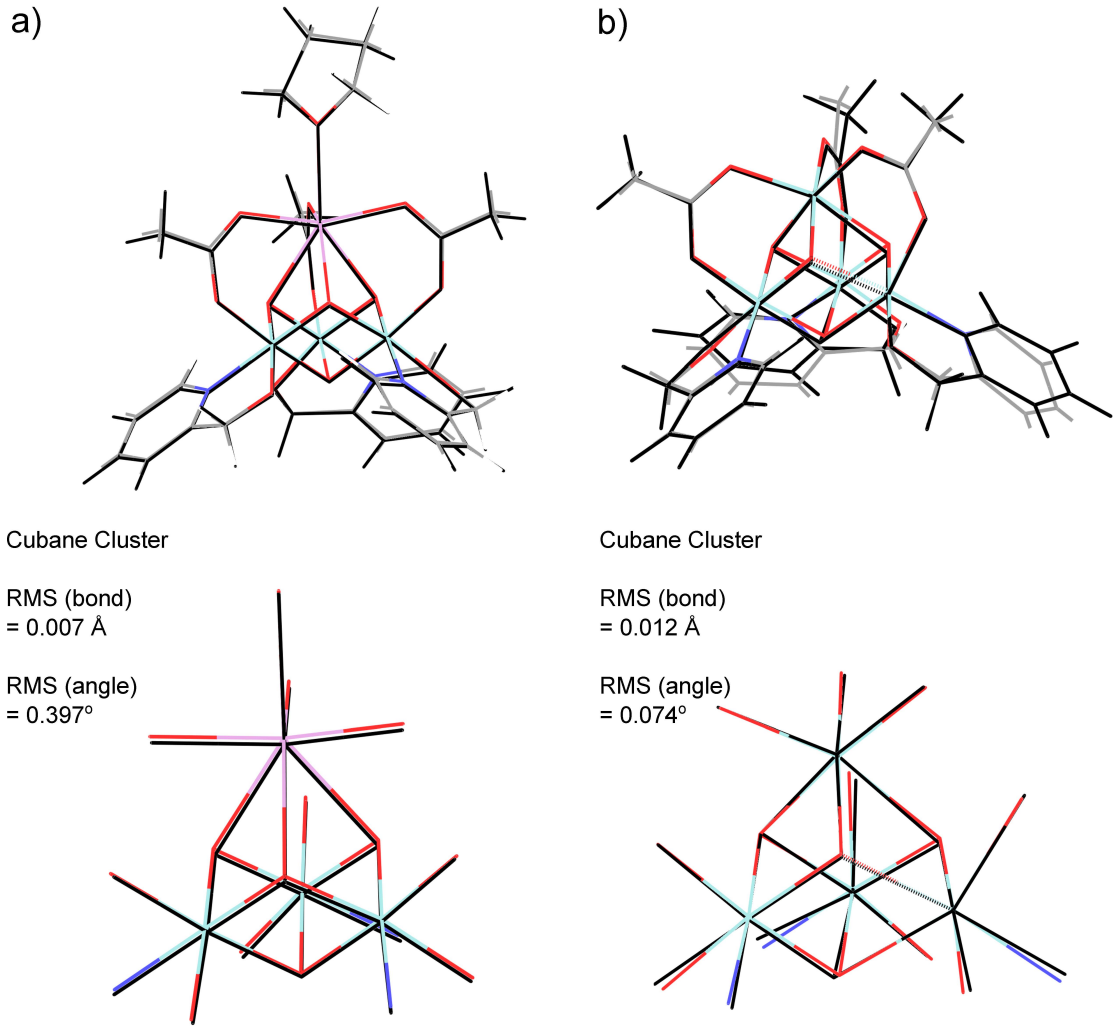

Figure S1: Comparison of geometries obtained from experiment (colored: Ca; magenta, Mn; light blue, O; red, C; grey, H; white) and theory (black) using the simplified ligand. The structures with this simplified ligand are almost identical to the ones obtained with the full ligand (**Figure 4**).

1.1.1 Initial interrogation of properties by model compounds of 2 and 4

The first simplification was done on the $CaMn_3O_4$ (**4**) containing compound as it is shown in Figure S1a. In the case of the simplified ligand we have 84 atoms while with the full ligand we treated 147 atoms. Since we are most interested in the estimation of the metallic core, we compared the geometry between this core including the first coordination shell and the XRD structure, and the RMS obtained is 0.007 Å for the estimation of bonds and RMS of 0.397° for the estimation of angles. This is basically the same accuracy as with the full ligand model.

We performed a similar simplification for the Mn_4O_4 (**2**) containing compound as it is shown in Figure S 1b. With the full ligand we treat 134 atoms while with this simplification on the ligand we only need to handle 71 atoms. In this case, we are also interested in how accurate we can predict the geometry of the Mn_4O_4 cluster and the first coordination shell, since we believe most of the electrochemical processes occur there. By comparing the experimental and the computational geometry of the cluster obtained with the simplified ligand the RMS is

0.012 Å for estimation of bonds and the RMS is 0.074° for the estimation of angles. This is practically the same as with the full ligand. With the simplified ligand we obtain a better estimation of the geometry for the Mn_4 case than for the $CaMn_3$ structure, including when only taking into account the cluster and its first coordination shell.

Thus, the models with the simplified ligand gives an accurate description of the geometry observed in experiments and speeds up our calculation by reducing the number of atoms to be treated to almost a half. We then put the full ligand into these models to obtain the final energies as shown below and in the main text.

1.2 Validation of the Computational Methodology: Redox Potential.

First we compared the accuracy of using the B3LYP and M06 [7] methodologies by benchmarking a single-electron redox potential in simple well characterized early transition metal (TM) complexes. We compare to experimental values and previous QM values in Table S1. We see that B3LYP leads to an average absolute error of 0.179 V, which is equivalent to an error of 4.1 kcal/mol, the normal range of accuracy for B3LYP. This compares to an RMS error of 0.292 V for M06 for the same basis set. We see that our basis set (including the two f-functions from [5] on each metal) performs 0.04 to 0.08 V better than the Dunning correlation-consistent triple-ζ basis set which includes a double set of polarization functions, cc-pVTZ-(-f)$^{++}$. [8] Thus we confirm that our level of QM is sufficiently accurate to estimate the redox potential for these early transition metal compounds.

Table S1: Redox potential performance for different transition metals using various QM methodologies (Relative to SHE)[a].

Compound	Sol.[b]	Ch[c]	E^0([9]) (exptl.)	B3LYP E^0([9]) cc-pVTZ(-f)$^{++}$	B3LYP E^0([d]) 6-311G^{**++}	M06 E^0([d]) cc-pVTZ(-f)$^{++}$	M06 E^0([d]) 6-311G^{**++}
$Fe(CpCOMe)_2$	DMF	+1/0	0.98	0.60	0.75	0.96	1.13
$FeCp_2$	AN	+1/0	0.55	0.67	0.81	0.06	0.26
$FeCp^*_2$	DMF	+1/0	0.14	0.19	0.25	-0.47	-0.33
$CoCp_2$	DMF	+1/0	-0.67	-0.76	-0.42	-0.75	-0.58
$Cr(BzMe_3)_2$	DMF	+1/0	-0.74	-1.11	-0.96	-1.34	-1.2
FeCpBz	DMF	+1/0	-1.12	-1.37	-1.14	-1.26	-1.15
$CoCp^*_2$	DMF	+1/0	-1.19	-1.34	-1.1	-1.35	-1.27
FeCpBz*	DMF	+1/0	-1.33	-1.58	-1.46	-1.61	-1.5
FeCp*Bz*	DMF	+1/0	-1.61	-1.67	-1.57	-1.69	-1.59
$CrCp^*_2$	AN	0/-1	-2.06	-2.22	-2.3	-2.85	-2.75
$MnCp^*_2$	AN	0/-1	-2.26	0.6	-2.42	0.96	1.13
			RMSD	0.211	0.179	0.373	0.292

[a] The conversion for QM is done by: $E^\circ = (\Delta G^\circ)/23.06 - 4.28$
[b] Solvent.
[c] charge.
[d] This work.

Next, we calculated the redox potential for the OEC models and then compare to our experimental values. We optimize the structures for the high spin state (S) of each compound Table S2 shows our calculated redox potential redox potential for the $CaMn_3O_4$ and Mn_4O_4 containing compounds. We see that B3LYP leads to an everage of absolute error of 0.21 V whereas M06 leads to 0.05V. This seems to be an artifact since the error

for Ferrocene ($FeCp_2$) redox potential (Table S1) is +0.26 V for B3LYP and -0.29 V for M06. Since the redox potential for the cubanes are referenced to Ferrocene, it may be that the lower error for M06 is due to cancellation of errors.

Table S2: Oxidation/reduction potentials for the Mn_3CaO_4 compound with respect to ferrocene/ ferrocenium. Solvents: dimethylacetamide (DMA) and dimethylformamide (DMF).

Compound	Solvent	$E°_{redox}$/V Exp	Total spin (S) used for QM	$E°_{redox}$/V B3LYP	$E°_{redox}$/V M06
$[Mn^{IV}{}_2Mn^{III}CaO_4]/[Mn^{IV}{}_3CaO_4]$	DMA	-0.94	(S =10/2)/(S =9/2)	-1.07	-0.84
$[Mn^{IV}{}_2Mn^{III}CaO_4]/[Mn^{IV}{}_3CaO_4]$	DMF	-0.89	(S =10/2)/(S =9/2)	-1.16	-0.92
$[Mn^{IV}{}_2Mn^{III}{}_2O_4]/[Mn^{IV}{}_3Mn^{III}O_4]$	DMA	+0.29	(S =14/2)/(S =13/2)	+0.11	+0.35
$[Mn^{IV}{}_2Mn^{III}{}_2O_4]/[Mn^{IV}Mn^{III}{}_3O_4]$	DMA	-0.70	(S =14/2)/(S =15/2)	-0.93	-0.67

The addition of a new electron affects the geometry of the $Mn^{IV}{}_3CaO_4$ and $Mn^{IV}{}_3Mn^{III}O_4$ compounds as it is shown in Figure S2. The extra electron reduces one of the Mn^{IV} to Mn^{III}, populating an e_g orbital that increases the bond distances along one axis.

For $Mn^{IV}{}_3CaO_4$, these bonds are the Mn_3-O_8 and the Mn_3-O_{16} bonds as shown in Figure S2. The changes are as follows: The oxidized compound has a Mn_3-O_8 bond distance of 1.91 Å, compared to a bond distance of 2.38 Å for the reduced system. The same elongation is found for the Mn_3-O_{16}, where the oxidized species has a bond distance of 1.93 Å, while the reduced one has a bond distance of 2.27 Å. Thus the reduced species has one bond distance at least 0.33 Å longer than the oxidized compound along one z-axis.

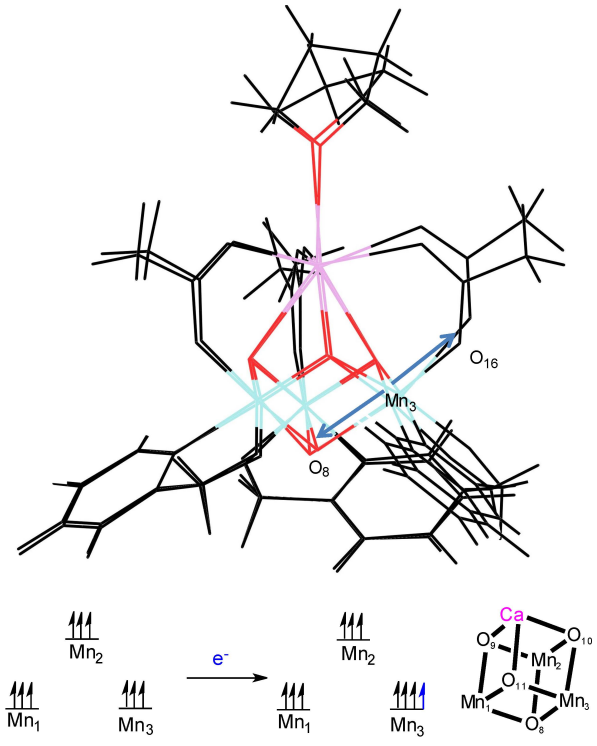

Figure S2: Oxidation/reduction for the Mn_3CaO_4 compound. Color code: Ca; magenta, Mn; light blue, O; red, C and H; black.

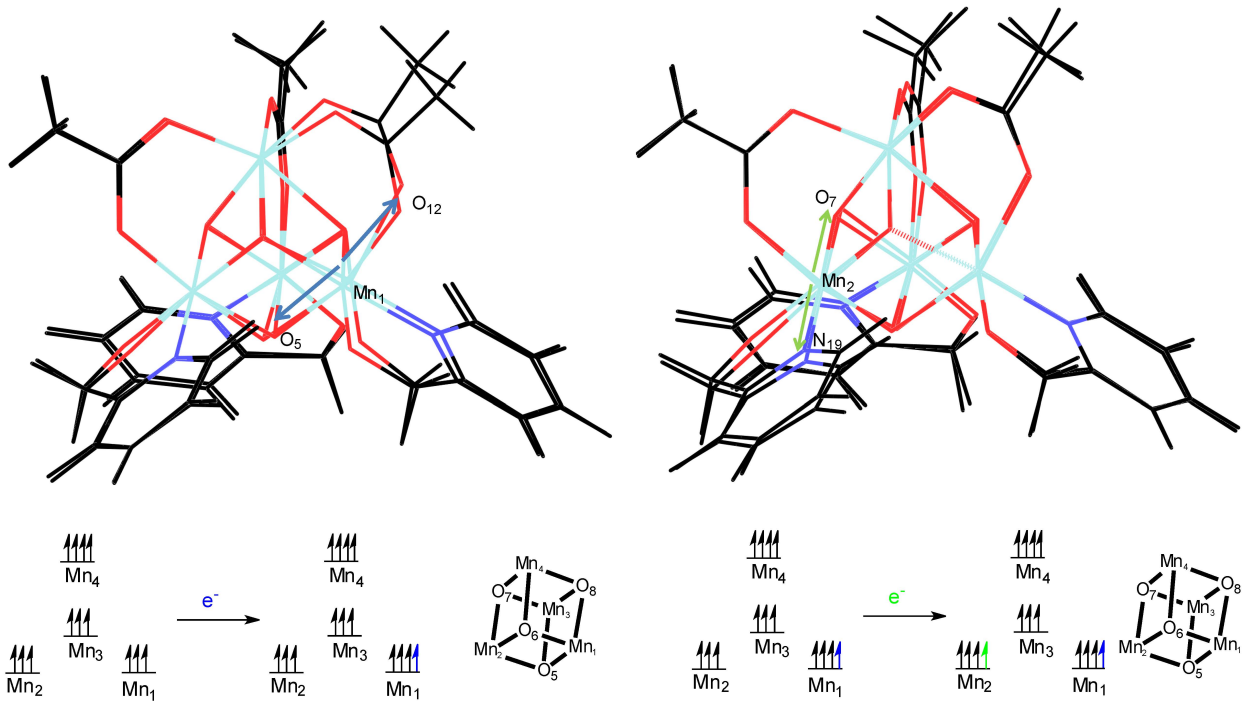

Figure S3: Oxidations/reductions for the Mn_4O_4 compound. Color code: Ca; magenta, Mn; light blue, O; red, N; dark blue, C and H; black

For $Mn^{IV}{}_3Mn^{III}O_4$ this elongation is in the bonds between Mn_1-O_5 which increase from 1.92 to 2.41 and Mn_1-O_{12}, which increase from 1.99 Å to 2.23 Å and one of its e_g orbitals is populated, changing the bond distance along that axis (Figure S3). This time the modified bonds are Mn_2-O_7 and Mn_2-N_{19}. The changes are as follows: Mn_2-O_7 bond distance increase from 1.85 Å to 2.21 Å when reduced, while the Mn_2-N_{19} increases from 2.07 Å to 2.29 Å.

Thus we have validated that the B3LYP QM provides a good description of the experimental redox potential for these systems. We also validated how reducing the Mn^{IV} atoms to Mn^{III} affects the geometry.

2 Transition States (TS)

2.1 Scan for the O-P bond formation

We located the Transition States (TS) for the reaction with PMe_3 on both high- and low-spin potential energy surfaces. The energy surface for the coordinate of the reaction [Cubane(O)-(P)Me_3 distance] is shown in Figure S4. After the scan was performed we picked the highest energy point structure with the lowest internal forces for the coordinate reaction ($<10^{-3}$ hartrees/bohr for the O-P bond) and we optimize for the transition state in order to obtain one and only one negative frequency. The surface for Mn_4O_4 (**2**) involving partial detachment of MeCOO- is similar to Figure S4.b.

The low spin transition state gives a higher barrier of at least 1 kcal/mol (See Table S3). In the main text we discuss barriers with the following spins: **4A**‡, S =11/2; **4B**‡, S =11/2; **2C**‡, S =16/2; **2D**‡, S =16/2; **2E**‡,

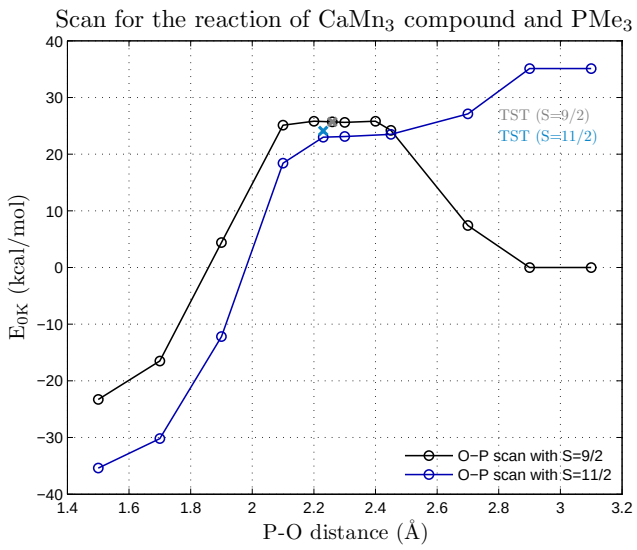

4.a: **4** reacting with PMe_3 ($\mathbf{2E}^{\ddagger}$)

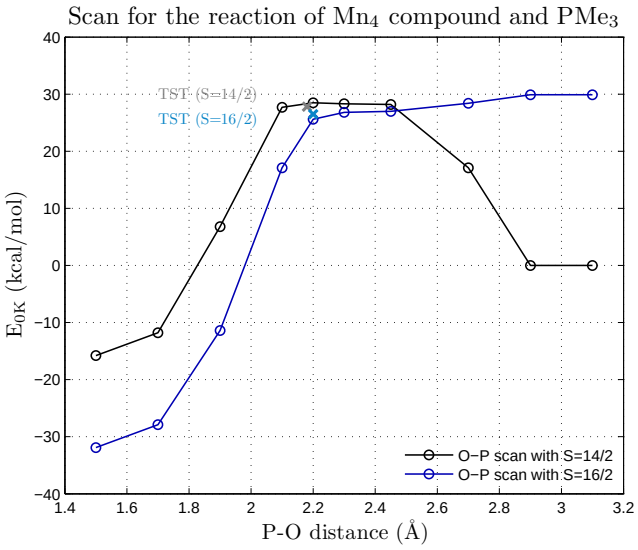

4.b: **2** reacting with PMe_3 ($\mathbf{4B}^{\ddagger}$)

Figure S4: Energy surface for the formation of the O-P bond when compound **4** (a) and **2** (b) react with PMe_3. The points marked as TST are the *a posteriori* optimization for transition state of the point with the lowest internal forces for the reaction coordinate.

S =16/2; $\mathbf{2F}^{\ddagger}$, S =16/2; and $\mathbf{2G}^{\ddagger}$, S =16/2. However the same conclusions can be obtained if we use the low-spin barriers. From Figure S4 we observe that using the spin-crossing point could be another way to represent the barriers, however in this energy surface we have used constrained the P-O bond in order to perform the scan, therefore, the spin crossing might be higher in energy. We discussed the high-spin energy surface but the same conclusions are obtained if either approach is used.

Table S3: Transition State barriers of reactions with PMe_3 with low- and high-spin energy surface. Energy: kcal/mol.

Compound	$\mathbf{2C}^{\ddagger}$	$\mathbf{2D}^{\ddagger}$	$\mathbf{2E}^{\ddagger}$	$\mathbf{2G}^{\ddagger}$	$\mathbf{2F}^{\ddagger}$[a]
2 ($S = 16/2$)	24.5	23.7	28.4	18.3	63.6
2 ($S = 14/2$)	34.7	36.8	29.7	27.3	68.4
Compound	$\mathbf{4B}^{\ddagger}$	$\mathbf{4B}^{\ddagger}$	$\mathbf{4B}^{\ddagger}$	$\mathbf{4B}^{\ddagger}$	$\mathbf{4A}^{\ddagger}$[b]
4 ($S = 11/2$)	28.7	28.7	28.7	N/A	90.2
4 ($S = 9/2$)	30.3	30.7	30.7	N/A	95.1

[a] This value is a barrier for the scan and it was not optimized for a transition state configuration.
[b] This value is a barrier for the scan and it was not optimized for a transition state configuration.

Accordingly, in Figure S5, we show the the high-spin transition state structures for **2** involving partial detachment of MeCOO-, and without allowing partial detachment of MeCOO-. We also include the high-spin transition state structure for **4** for which we did not observe partial detachment of MeCOO-.

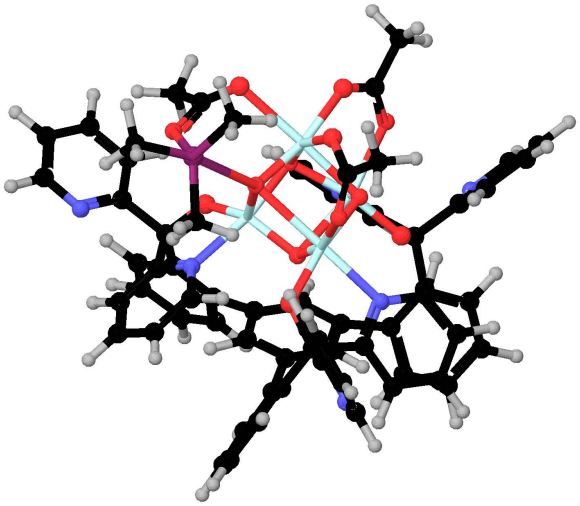

5.a: Transition State $\mathbf{2G}^{\ddagger}$

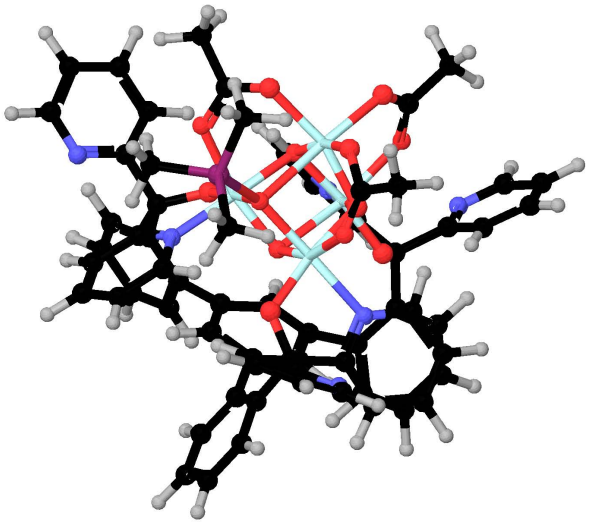

5.b: Transition State $\mathbf{2C}^{\ddagger}$

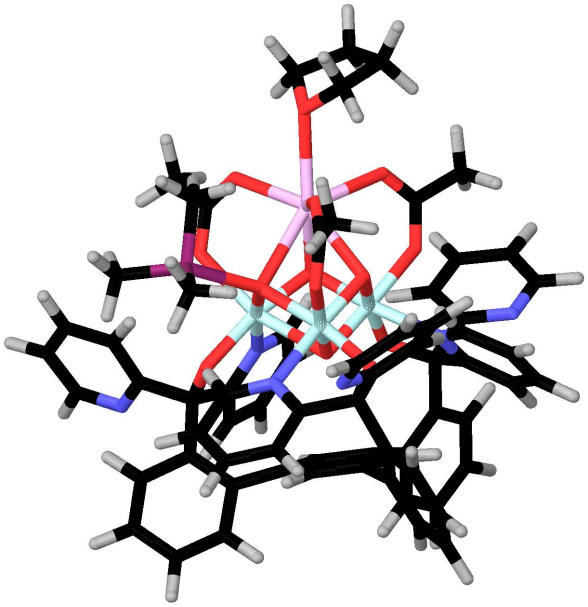

5.c: Transition State $\mathbf{4B}^{\ddagger}$

Figure S5: Transition States for reactions of **2** and **4** with PMe_3. (a) Transition state of Mn_4O_4 involving partial detachment of MeCOO-($\mathbf{2G}^{\ddagger}$) (b) Transition state of Mn_4O_4 without allowing partial detachment of MeCOO-($\mathbf{2C}^{\ddagger}$), which is very similar to $\mathbf{2D}^{\ddagger}$ and $\mathbf{2E}^{\ddagger}$. (c) Transition state of Mn_3CaO_4 ($\mathbf{4B}^{\ddagger}$).

2.2 TS with Partial detachment of MeCOO- in Mn_4O_4 (2)

Table S4: Atomic coordinates transition state with partial detachment of MeCOO- in **2**

	x	*y*	*z*
Mn1	14.44031689	-0.252114469	12.10708984
Mn2	11.6707815	0.046376483	13.38066833
Mn3	13.51630797	2.405939478	13.08558062
Mn4	14.1603268	0.158338229	14.9473416
O5	12.52461629	1.210401746	12.21309459
O6	13.23434091	-0.975649324	13.32869024
O7	12.88693996	1.460319346	15.02895417
O8	14.88007905	1.116596392	13.4226266
O12	16.12285935	-1.499488741	12.92584045
O13	15.72833855	-1.017361947	15.09953594
O14	11.11457234	-1.054250001	15.05606291
O15	13.10997805	-1.163029372	16.13000042
O16	13.88036699	3.306585397	16.78723272
O17	15.21387424	1.479556878	16.59476951
C120	16.38041434	-1.583983659	14.14694367
C121	17.56694328	-2.423146103	14.59765074
H122	18.06743197	-2.875326796	13.74019625
H123	17.22238537	-3.203767795	15.28370069
H124	18.27177429	-1.792997845	15.15033385
C125	11.92193104	-1.561729859	15.88495024
C126	11.44667988	-2.769182907	16.67451736
H127	11.77137319	-3.669305535	16.13959214
H128	10.3573214	-2.785366941	16.74091825
H129	11.89999062	-2.790918866	17.66827536
C130	15.05264903	2.67038997	16.43327916
C131	16.0366491	3.627540541	15.8447604
H132	15.97516732	4.609991802	16.31666593
H133	15.78117697	3.742495549	14.78127028
H134	17.04005841	3.209210612	15.92622592
P85	12.46310161	2.528194112	17.20078678
C73	10.9019621	2.714909388	16.2894435

Continued on next page

Table S4 – *Continued from previous page*

	x	y	z
H74	10.71047687	1.851283175	15.6589219
H88	10.11509723	2.878390027	17.03431745
H76	10.98047431	3.60422794	15.66217032
C77	12.14422559	3.743908591	18.56237732
H91	11.99732085	4.743321881	18.14210402
H92	11.24623472	3.465379367	19.12211904
H93	12.99460527	3.780342001	19.24785896
C94	12.67619303	1.00786617	18.16491977
H95	13.46277855	1.189728498	18.90129036
H96	11.72726669	0.849007678	18.690107
H97	12.92171341	0.140450048	17.55620921
O9	13.97118884	-1.203639287	10.55249346
O10	9.97549477	0.971602323	13.21783622
O11	14.68333053	3.861905178	12.59825705
N18	15.79295043	0.589269792	10.77495801
N20	10.58627223	-1.196271531	11.85699449
N22	12.13840488	4.016553456	13.04333475
C24	16.61532792	1.617963563	11.04245098
H25	16.52719213	2.030749617	12.04116517
C26	17.48376213	2.117140825	10.08156339
H27	18.13384288	2.952671848	10.31947233
C28	17.48641889	1.531316827	8.812721308
H29	18.14915148	1.904893346	8.03649609
C30	16.62997712	0.468623078	8.546104576
H31	16.60535619	-0.015659776	7.579004735
C32	15.786832	0.013073367	9.562324896
C33	14.81808405	-1.171042186	9.443328397
C53	11.05953011	-2.276841055	11.21986932
H54	11.99679742	-2.667066862	11.60119385
C55	10.40289328	-2.832856512	10.12822333
H56	10.8098893	-3.708539824	9.633084327
C57	9.22943777	-2.221478921	9.679423405
H58	8.692722117	-2.622442478	8.823302812
C59	8.756762398	-1.085818469	10.32904314

Continued on next page

Table S4 – *Continued from previous page*

	x	y	z
H60	7.848144665	-0.588802025	10.01522494
C61	9.471521246	-0.596193149	11.42871929
C62	9.000449922	0.593311008	12.29568239
C82	10.80649779	3.91221287	13.23755737
H83	10.42745528	2.910339225	13.43224199
C84	9.962976782	5.006850093	13.10560591
H85	8.895455999	4.880679264	13.25269978
C86	10.50923305	6.233982852	12.72008421
H87	9.874553574	7.107466423	12.59504171
C88	11.87058164	6.316115129	12.45683348
H89	12.3243241	7.236562448	12.11436999
C90	12.66789666	5.180178948	12.63153538
C91	14.15967273	5.117760679	12.28225276
N19	6.753926746	-0.504984626	12.37653037
N21	14.31872787	7.089779322	13.82131043
N23	16.78348819	-2.474377527	8.644515772
C34	7.785072183	-0.012011664	13.08085572
C35	7.8280316	-0.074892098	14.47598605
H36	8.701563808	0.305991643	14.98616521
C37	6.75800864	-0.653702194	15.15655348
H38	6.768404488	-0.716522622	16.24227435
C39	5.681709299	-1.15689304	14.4290533
H40	4.828731679	-1.61853793	14.91775916
C41	5.734987505	-1.05929088	13.03863116
H42	4.920055166	-1.445429256	12.42672274
C43	8.550564081	1.810960679	11.40584414
C44	7.276745874	2.353861661	11.65397438
H45	6.665385415	1.919328146	12.43318177
C46	6.737256341	3.420472044	10.93834914
H47	5.740137243	3.780818135	11.17992108
C48	7.476554368	3.994305283	9.911638279
H49	7.075611284	4.807559806	9.31239534
C50	8.758446512	3.511114662	9.67230386
H51	9.354343096	3.969070957	8.888082359

Continued on next page

Table S4 – *Continued from previous page*

	x	y	z
C52	9.343091131	2.45418663	10.40327449
C63	14.96093469	6.138369887	13.13752519
C64	16.35851957	5.998801212	13.18984257
H65	16.82881748	5.20213925	12.62585799
C66	17.09791694	6.885555709	13.96096313
H67	18.18128544	6.806327635	14.00527781
C68	16.42619884	7.878785908	14.68126161
H69	16.96240726	8.591617492	15.30069119
C70	15.04086908	7.931332899	14.57918397
H71	14.47418613	8.685296599	15.12414315
C72	14.29676104	5.445652515	10.74476411
C111	14.95423703	6.635155091	10.38464065
H112	15.31006351	7.300580724	11.16169185
C75	15.18407857	7.012946447	9.062748714
H114	15.70023008	7.946168276	8.851499591
C115	14.75087374	6.186931369	8.033859652
H78	14.91880251	6.449197547	6.99275323
C79	14.06766631	5.019411815	8.361607022
H80	13.6905309	4.387449225	7.562709725
C81	13.80366619	4.620920227	9.687318429
C92	15.70127366	-2.454157656	9.435993783
C93	15.35000967	-3.530500061	10.25454749
H94	14.47802354	-3.442441803	10.88882598
C95	16.1499278	-4.669899585	10.23986505
H125	15.90043799	-5.522383801	10.8665721
C97	17.27759345	-4.697365718	9.419985227
H98	17.93264988	-5.562758374	9.382302857
C99	17.549429	-3.571455774	8.645425301
H100	18.42098672	-3.546469847	7.991890853
C101	13.96539088	-1.051289685	8.146394039
C102	14.10963326	-2.000952273	7.124267839
H103	14.84581448	-2.786765412	7.230850414
C104	13.34273111	-1.973344352	5.960548967
H105	13.49365684	-2.732939873	5.197698017

Continued on next page

Table S4 – *Continued from previous page*

	x	*y*	*z*
C106	12.39285952	-0.974061546	5.791089485
H107	11.78260001	-0.927575842	4.89249403
C108	12.2317645	-0.023390422	6.794497027
H109	11.49442462	0.764624773	6.668280977
C110	12.99398284	-0.029452285	7.977109775
C139	12.6312651	1.086293687	8.921156095
C112	11.31066737	1.12312942	9.401002971
H113	10.67064097	0.270671842	9.211418525
C114	10.79647077	2.253401134	10.03964735
C143	11.63562626	3.377412193	10.16582185
H116	11.21238294	4.295407861	10.5560202
C117	12.97216067	3.361073243	9.754409131
C118	13.4519955	2.201133062	9.118455436
H119	14.45661881	2.209227375	8.709226877

2.3 TS without Partial detachment of MeCOO- for Mn_4O_4 (2)

Table S5: Atomic coordinates transition state without partial detachment of MeCOO- in **2**

	x	*y*	*z*
P85	12.2290628994	1.4425661024	17.0715524261
C73	12.92754601	0.272335873	18.26921174
H74	14.01057239	0.392981172	18.3015655
H88	12.47597111	0.463368645	19.25004873
H76	12.72563139	-0.745246687	17.93044214
C77	10.42742832	1.249402982	17.02708582
H91	10.20058408	0.320886176	16.49621178
H92	10.02083696	1.225352792	18.04411056
H93	9.987896441	2.0765942	16.46891489
C94	12.70283847	3.135040829	17.53219407
H95	12.12277555	3.850581371	16.94667283
H96	12.52764896	3.291528721	18.60270358

Continued on next page

Table S5 – *Continued from previous page*

	x	y	z
H97	13.76048558	3.272193515	17.29202607
Mn1	14.75876995	-0.2956221	12.08852278
Mn2	11.9676280550	0.2113856389	13.2800022131
Mn3	14.2326509353	2.1761499300	13.8826350233
Mn4	14.4175370807	-0.7253223315	14.8416340040
O5	13.24106434	1.453325868	12.56857901
O6	13.35925269	-1.04811592	13.24118896
O7	12.8432324716	1.1111665973	15.0485422388
O8	15.36477302	0.403538832	13.73908263
O9	14.14429885	-0.741977649	10.38201734
O10	10.47719396	1.353427525	13.11923406
O11	15.21241547	3.541194767	12.91656561
O12	16.00288166	-2.084057901	12.40282488
O13	15.72176688	-2.351946618	14.63025996
O14	11.13977537	-1.212023717	14.8216897
O15	13.06289579	-1.771795551	15.89723063
O16	15.3581121	2.403416567	15.65902383
O17	15.36647904	0.256173507	16.40798177
N18	16.2236362	0.633258952	10.97778211
N20	10.85478172	-0.824436617	11.78455081
N22	12.87403999	4.03382532	14.01573875
C24	17.16901117	1.457025462	11.45583402
H25	17.14593932	1.619069948	12.52727497
C26	18.09359814	2.058822111	10.61355377
H27	18.84537063	2.726410794	11.02082816
C28	18.01742131	1.798123925	9.24327935
H29	18.72138084	2.261210892	8.556975666
C30	17.03330873	0.941771151	8.759809871
H31	16.94681139	0.712399074	7.7052886
C32	16.14128468	0.365340964	9.66351639
C33	15.04175305	-0.642989616	9.309182536
C53	11.26156529	-1.918068582	11.12239837
H54	12.19347704	-2.348932018	11.47169844
C55	10.53618814	-2.431838	10.05557009

Continued on next page

Table S5 – *Continued from previous page*

	x	y	z
H56	10.88793953	-3.314938931	9.532475488
C57	9.366885341	-1.773844619	9.665835534
H58	8.781921943	-2.142901592	8.827573275
C59	8.9561969	-0.640362451	10.35878088
H60	8.054407467	-0.105550223	10.08481788
C61	9.73011356	-0.189654132	11.42855645
C62	9.378151633	1.007001162	12.32091555
C82	11.57314543	4.091669011	14.34566585
H83	11.1168486	3.141881924	14.60392575
C84	10.8377117	5.267714939	14.27422191
H85	9.784176311	5.274237767	14.53709533
C86	11.482006	6.425149106	13.82515962
H87	10.94375077	7.367176212	13.75929093
C88	12.8086646	6.346071386	13.423794
H89	13.33217996	7.207536532	13.03011631
C90	13.47387378	5.115227351	13.51461418
C91	14.91834078	4.890219291	13.00926864
C120	16.22208709	-2.666323598	13.50105417
C121	17.19085049	-3.841987478	13.49546252
H122	17.3079992	-4.241130732	12.48645759
H123	16.84681601	-4.620720625	14.18084492
H124	18.16803674	-3.494679917	13.85118674
C125	11.83649613	-1.959627125	15.55303868
C126	11.19443522	-3.217267772	16.11822549
H127	11.50958593	-4.064089852	15.49731982
H128	10.10567553	-3.147685624	16.08609938
H129	11.54395779	-3.412485215	17.13537705
C130	15.81575853	1.449273745	16.35798105
C131	17.01184408	1.753154446	17.24495787
H132	17.13292	2.828312713	17.38599117
H133	17.90600711	1.359930215	16.74738166
H134	16.92463249	1.23936091	18.20586384
N19	7.5685844	-0.557905961	13.04733284
N21	15.49848893	6.673447371	14.65973603

Continued on next page

Table S5 – *Continued from previous page*

	x	*y*	*z*
N23	16.94539082	-2.041492536	8.531864862
C34	8.24325623	0.568168602	13.2902167
C35	7.971396549	1.3750136	14.40623573
H36	8.534287792	2.291083456	14.541211
C37	6.972681389	0.991381452	15.29034017
H38	6.729558283	1.608414284	16.15237807
C39	6.278903915	-0.198610903	15.04969426
H40	5.49243183	-0.541628465	15.71524087
C41	6.616911318	-0.930973696	13.91715609
H42	6.098537912	-1.85992345	13.68419152
C43	8.909905268	2.229577769	11.46875943
C44	7.540600324	2.544906174	11.43898945
H45	6.836145047	1.898869659	11.95035432
C46	7.037282472	3.669472279	10.78658057
H47	5.968116227	3.865552158	10.79691721
C48	7.914615428	4.532562795	10.13995151
H49	7.553460105	5.4246697	9.635179473
C50	9.270350526	4.217686654	10.12282257
H51	9.958295705	4.858690507	9.578882087
C52	9.800146228	3.07313886	10.75038696
C63	15.8819496	5.54898633	14.03961737
C64	17.1235483	4.949849076	14.2800875
H65	17.36303603	4.031362569	13.76084373
C66	17.99525713	5.546996268	15.18392936
H67	18.96989716	5.107314427	15.38126304
C68	17.59887142	6.716479016	15.8360277
H69	18.2450594	7.214808141	16.55282552
C70	16.34070558	7.233187251	15.53920014
H71	15.9887522	8.143275913	16.02422905
C72	15.06104869	5.566359068	11.60743996
C111	15.8758072	6.698575837	11.45416517
H112	16.37189778	7.116439924	12.32174043
C75	16.07664975	7.319708162	10.22126228
H114	16.71944982	8.194329128	10.15723903

Continued on next page

Table S5 – *Continued from previous page*

	x	y	z
C115	15.45267763	6.811164521	9.088091923
H78	15.59128329	7.275786698	8.11532126
C79	14.63481863	5.69120384	9.220532026
H80	14.13292267	5.291832448	8.343345078
C81	14.41402241	5.049404141	10.45351806
C92	15.72855206	-2.020261031	9.087875836
C93	15.04378628	-3.185245551	9.445835138
H94	14.06905705	-3.098992564	9.907512442
C95	15.6478649	-4.414790573	9.210367844
H125	15.13813161	-5.337594041	9.475688799
C97	16.92133002	-4.445426284	8.638814437
H98	17.43366987	-5.382856979	8.443514568
C99	17.52502963	-3.231469504	8.323146397
H100	18.51834371	-3.206583083	7.876645758
C101	14.2723649	-0.215206362	8.028661046
C102	14.4739453	-0.911236508	6.826782545
H103	15.204104	-1.709917647	6.790571256
C104	13.76548072	-0.613365887	5.663994139
H105	13.9564632	-1.180018253	4.756199357
C106	12.81630177	0.401601155	5.682644638
H107	12.24500776	0.64869434	4.79131106
C108	12.61405534	1.11342059	6.861366682
H109	11.8933824	1.926398326	6.878791031
C110	13.32904591	0.841579989	8.04174068
C139	13.01013256	1.776044453	9.173445649
C112	11.69634485	1.822739336	9.662318381
H113	10.9870929	1.07388423	9.32519043
C114	11.2650477	2.866439807	10.48734036
C143	12.17428084	3.886566808	10.81369178
H116	11.8185712	4.739605073	11.38142274
C117	13.49628076	3.859116559	10.35784812
C118	13.89660019	2.794444002	9.53485141
H119	14.89586614	2.811193085	9.112043683

2.4 TS for Mn_3CaO_4 (4)

Table S6: Atomic coordinates transition state in **4**

	x	y	z
Mn1	-1.3148584541	3.4940628685	24.2931256325
Mn2	-0.647302529	2.087654526	26.81231646
Mn3	1.5355016182	3.0680800496	25.4028827947
Ca4	0.0014229056	0.3855946951	24.1060662276
O5	-1.180445673	5.282438812	23.65026071
O6	-2.020229184	2.832720594	27.87996741
O7	2.636395884	3.545250238	26.8600596
O8	0.00291282	3.693588482	26.16868101
O9	-1.573075626	1.921044388	25.24302465
O10	0.955769003	1.481760257	26.0509097
O11	0.5404491560	2.8522090819	23.7374379983
O12	-2.261283322	2.680853503	22.48328564
O13	-1.683355832	0.504836733	22.38898827
O14	-1.19205308	0.246409101	27.43471837
O15	-0.780907993	-1.179495923	25.72753205
O16	3.179440336	2.210052629	24.51696614
O17	2.40320817	0.21599181	23.78184244
O18	0.334787333	-1.86102481	22.90184295
N19	-3.063623781	4.312056714	25.07158929
N20	0.277345693	2.085747625	28.70247789
N21	2.292642187	4.968402404	24.76629509
N22	-4.163501067	7.140008534	22.64249063
N23	-2.542704602	0.752289151	30.77998196
N24	5.938097883	4.248646911	25.680086
C25	-3.955483825	3.631415939	25.80823167
H26	-3.733467273	2.577897987	25.92944468
C27	-5.056963146	4.258039346	26.37504736
H28	-5.764441606	3.684651144	26.96467397
C29	-5.210666535	5.634049575	26.19159904

Continued on next page

Table S6 – *Continued from previous page*

	x	*y*	*z*
H30	-6.052189203	6.157572205	26.63761878
C31	-4.278897805	6.332785825	25.43168868
H32	-4.373636121	7.394369774	25.24566974
C33	-3.20921677	5.632036877	24.87008489
C34	-2.204623921	6.212373952	23.87102654
C35	-3.063772812	6.374494922	22.57317567
C36	-2.686925478	5.712846861	21.40600865
H37	-1.81428465	5.078819996	21.43129041
C38	-3.469600692	5.87080214	20.26337348
H39	-3.198321046	5.367588	19.33836496
C40	-4.605308366	6.674894778	20.32464629
H41	-5.244360398	6.825093203	19.45958081
C42	-4.909398184	7.281568048	21.54353239
H43	-5.792265001	7.912510153	21.64186021
C44	-1.598510953	7.586969841	24.29936649
C45	-1.663349854	8.650510338	23.38133476
H46	-2.158209466	8.500603246	22.43167094
C47	-1.122587139	9.909084936	23.62983855
H48	-1.211251402	10.69101655	22.87989591
C49	-0.485709501	10.1491513	24.8405484
H50	-0.070786849	11.12645351	25.074104
C51	-0.379739305	9.107808176	25.75437401
H52	0.127091649	9.281418819	26.69908319
C53	-0.898637117	7.818419166	25.51813635
C54	1.551056257	1.74567691	28.94182447
H55	2.132690079	1.503229914	28.06175613
C56	2.063565235	1.725377744	30.23291369
H57	3.100335251	1.452163131	30.40106452
C58	1.223673481	2.073616064	31.29298463
H59	1.597184666	2.078650097	32.31370794
C60	-0.100967969	2.407183453	31.03189662
H61	-0.78844261	2.66821586	31.82618464
C62	-0.549195889	2.391198596	29.71016511
C63	-1.990459556	2.651673066	29.26731915

Continued on next page

Table S6 – *Continued from previous page*

	x	y	z
C64	-2.850858756	1.416329482	29.66100544
C65	-3.966747016	1.091763873	28.88107664
H66	-4.154622555	1.656652161	27.9779818
C67	-4.794056615	0.05355858	29.29175057
H68	-5.673666106	-0.212396608	28.71040044
C69	-4.477363274	-0.644290786	30.46061372
H70	-5.095005447	-1.462487096	30.81904815
C71	-3.336922018	-0.259247827	31.15890535
H72	-3.046112122	-0.776905276	32.07230533
C73	-2.56871563	3.910910958	29.98554229
C74	-3.535918358	3.772900678	30.99435241
H75	-3.856081952	2.785017898	31.29933696
C76	-4.108423165	4.871294749	31.63436866
H77	-4.85234034	4.713457487	32.41129079
C78	-3.726234065	6.156517484	31.26830556
H79	-4.163279613	7.027932916	31.74940447
C80	-2.761719846	6.313180709	30.27775558
H81	-2.441674071	7.311323268	29.99272926
C82	-2.162212722	5.218667774	29.63194112
C83	1.800036509	5.77388647	23.80760859
H84	0.858383648	5.46967346	23.36482095
C85	2.41373763	6.974473514	23.47371362
H86	1.969210278	7.613132721	22.71717011
C87	3.57820573	7.345325006	24.1504027
H88	4.088843204	8.273602357	23.90748544
C89	4.050959233	6.533126016	25.17370479
H90	4.920619162	6.804011346	25.75814564
C91	3.362008124	5.355648903	25.47637073
C92	3.671176859	4.467984529	26.68317598
C93	5.009157701	3.713814187	26.47857874
C94	5.228085936	2.53369192	27.20113838
H95	4.433667038	2.147824443	27.82730605
C96	6.460751693	1.901817515	27.09754927
H97	6.663771553	0.993616932	27.66021746

Continued on next page

Table S6 – *Continued from previous page*

	x	y	z
C98	7.43504429	2.452706639	26.26011705
H99	8.412282872	1.992676895	26.14684801
C100	7.118061157	3.618742978	25.57072312
H101	7.84556543	4.082394716	24.90553706
C102	3.775717461	5.38027006	27.95105253
C103	5.02944932	5.591899652	28.54732267
H104	5.912495041	5.14361981	28.10897927
C105	5.192586147	6.363251176	29.69670267
H106	6.184716482	6.496141216	30.1207685
C107	4.080958282	6.948678576	30.28998439
H108	4.179479153	7.549477762	31.19063442
C109	2.831633279	6.764148247	29.70571441
H110	1.95958841	7.235729359	30.15023686
C111	2.64319148	6.003074185	28.53785346
C112	1.219540974	5.97510556	28.05885481
C113	0.242068988	5.429952252	28.90242819
H114	0.553150997	4.927632914	29.81258129
C115	-1.117114273	5.582633304	28.62407317
C116	-1.505935718	6.304522607	27.48777004
H117	-2.561370489	6.48131813	27.32384878
C118	-0.559575238	6.84981975	26.61865041
C119	0.802008242	6.689290136	26.93400122
H120	1.539145631	7.184371245	26.31313779
C121	-2.462667606	1.472732682	22.14587234
C122	-3.753416343	1.172603914	21.39134311
H123	-3.612363074	0.341781122	20.69559681
H124	-4.116326483	2.058990099	20.86670619
H125	-4.517375414	0.874182379	22.11985881
C126	-1.163921115	-0.911959238	26.89228968
C127	-1.639165718	-2.040433547	27.79833785
H128	-1.703489261	-2.980864306	27.24834355
H129	-2.611163562	-1.788056923	28.23038043
H130	-0.936402129	-2.15277708	28.63103043
C131	3.325450961	1.015477067	24.07695252

Continued on next page

Table S6 – *Continued from previous page*

	x	*y*	*z*
C132	4.768225751	0.56259025	23.90051659
H133	4.823566044	-0.289164644	23.21986247
H134	5.160698228	0.262040365	24.87819545
H135	5.39306526	1.384624785	23.54275586
C136	-0.815918453	-2.647154518	22.53465735
H137	-0.632602861	-3.098387998	21.54749311
H138	-1.660588067	-1.96094826	22.4583683
H141	-1.6399134	-3.406928295	24.39958285
H144	0.485100642	-3.508673273	25.27083917
C151	-0.936506084	-3.726641255	23.62820197
H152	-1.283183177	-4.678154876	23.21318039
C154	0.498735453	-3.816527317	24.22339072
H156	0.923862417	-4.823057134	24.15965509
C157	1.305642432	-2.807770399	23.38609882
H158	2.061493376	-2.243205685	23.93344876
H159	1.783833463	-3.296555694	22.52317874
P85	1.1402946757	3.1668467168	21.6034035632
C86	1.139667301	1.430114409	21.00977327
H87	0.12312138	1.027883249	21.03580552
H151	1.527671317	1.387075077	19.98573358
H89	1.775725	0.822832713	21.65953313
C90	2.918316427	3.645640082	21.5923129
H91	3.394731868	3.283849805	22.5054422
H92	3.412278227	3.216546939	20.71275519
H93	3.008495482	4.733556336	21.56067101
C158	0.443494908	4.087455631	20.14648434
H160	0.41738407	5.15992824	20.35576484
H96	1.05022024	3.909499268	19.24950094
H161	-0.576903123	3.739347142	19.9679519

Part II

Experiment

3 General Considerations

Reactions performed under inert atmosphere were carried out in a glovebox under a nitrogen atmosphere. Anhydrous tetrahydrofuran (THF) was purchased from Aldrich in 18 L Pure-Pac^{TM} containers. Anhydrous dichloromethane, diethyl ether, and THF were purified by sparging with nitrogen for 15 minutes and then passing under nitrogen pressure through a column of activated A2 alumina (Zapp's). Anhydrous N,N-dimethylformamide (DMF) was purchased from Aldrich and stored over molecular sieves. 97% H_2 ^{18}O was purchased from Aldrich and degassed by three freeze-pump-thaw cycles or sparging with N_2 for 10 minutes. NMR solvents were purchased from Cambridge Isotope Laboratories, Inc. Benzene-d_6 was vacuum distilled from sodium benzophenone ketyl. CD_2Cl_2 was dried over calcium hydride, then degassed by three freeze-pump-thaw cycles and vacuum-transferred prior to use. Celite was activated by heating under vacuum at 200 °C for 12 h. ^{1}H NMR and ^{31}P NMR spectra were recorded on a Varian 300 MHz instrument, with shifts reported relative to the residual solvent peak (^{1}H) or a phosphoric acid external standard (^{31}P). Elemental analyses were performed by Midwest Microlab, LLC, Indianapolis, IN. Electrospray Ionization Mass Spectrometry was performed in the positive ion mode using an LCQ ion trap mass spectrometer (Thermo) at the California Institute of Technology Mass Spectra Facility.

Unless indicated otherwise, all commercial chemicals were used as received. Tetrabutylammonium permanganate, [10] iodosobenzene, [11] and $Mn(OTf)_2{\cdot}CH_3CN$ [12] were prepared according to literature procedures. Tetra butylammonium acetate-d_3 (nBu4N$^+$ $O_2CCD_3^-$) was made by neutralization of a 1.0M nBu$_4$NOH solution in methanol (Sigma-Aldrich) with d_4-acetic acid (Cambridge) and removal of volatiles under vacuum at 40-50 °C over six hours. **Caution!** Tetrabutylammonium permanganate and iodosobenzene are potentially explosive and should be used only in small quantities.

4 Synthetic Procedures

4.1 Synthesis of 1,3,5-Tris(2-di(2'-pyridyl)hydroxymethylphenyl)benzene (H_3L).

Improving upon the published procedures, [13,14] in the glovebox, a 1L Erlenmeyer flask was equipped with a stir bar and charged with 1,3,5-tris(2- bromophenyl)benzene (8.83 g, 16.26 mmol) and Et_2O (325 mL). The off-white suspension was frozen in the cold well. While thawing, t-BuLi (1.7 M in pentane, 59 mL, 100 mmol) was poured in quickly. The mixture was stirred 1.5 hours as it came to room temperature. The solution flashes green immediately upon t-BuLi addition, followed by yellow. As it warmed, the solution became dark red and homogeneous, then light orange/pink and heterogeneous. The mixture was refrozen in the cold well. While thawing, a solution of di(2-pyridyl)ketone (8.98 g, 48.8 mmol) in 2:1 Et_2O/THF (70 mL) was added. The solution turned dark yellow and thick. The reaction mixture was allowed to warm to room temperature and stirred for 8 h under nitrogen. The mixture was taken out of the glovebox and poured into water (≈500 mL). The resulting orange solid was collected by filtration and washed with water and Et_2O. The solid was dissolved in CH_2Cl_2 and extracted twice with water and once with brine and dried over magnesium sulfate, then filtered. The solvent was removed under reduced pressure, and the yellow-orange solid was precipitated from acetone to yield the product as a white solid

(9.64 g, 69%). Spectral features match those found in previous work. [13, 14]

4.2 Synthesis of $LMn^{II}_3(OAc)_3$ (1).

Improving upon the published procedure, [14] under an N_2 atmosphere a solid mixture of **H3L** (8.64g, 10.0 mmol) and $Mn(OAc)_2$ (5.22g, 30.2 mmol) was suspended in degassed H_2O (15mL) and CH_3CN (65 mL). A solution of KOH (1.7g, 30.2 mmol) in degassed H_2O (10 mL) was added to the tan suspension under stirring. Over approximately thirty minutes, the solution became more clear and yellow, but never became fully homogeneous. If stirring was stopped, two liquid layers became visible: the top, dark yellow CH_3CN layer and clear and colorless bottom H_2O layer. After stirring for five hours, the reaction mixture was filtered through celite to remove a small amount of brown solid. The clear and colorless bottom layer was separated by pipette from the clear and yellow top layer to remove a majority of the KOAc side product. The CH_3CN solution was concentrated *in vacuo* to give a yellow powder. $CHCl_3$ (≈20 mL) was added and removed *in vacuo* twice to remove any CH_3CN and H_2O. The yellow powder was dissolved in $CHCl_3$, filtered through Celite, and Et_2O was vapor diffused into the $CHCl_3$ solution to afford yellow crystals of **1** (10.77g, 81% for **1**·$CHCl_3$). $CHCl_3$ could be removed by triturating **1**·$CHCl_3$ in THF for ≈3 hours and collecting the yellow solid by filtration (10.00g, 78% for **1**·THF). Spectral features match those found in previous work. [14]

4.3 Synthesis of $LMn^{III}_2Mn^{IV}_2O_4(OAc)_3$ (2).

4.3.1 Method A from $LMn^{II}_3(OAc)_3$: [15]

In the glovebox, yellow solid 1·$CHCl_3$ (57.8 mg, 0.045 mmol) and $n$$Bu_4NMnO_4$ (34.9 mg, 0.10 mmol) were separately dissolved in CH_2Cl_2 (≈4 mL) in scintillation vials. The purple solution of $n$$Bu_4NMnO_4$ was transferred to the stirring yellow solution of $LMn_3(OAc)_3$. The reaction mixture was stirred at RT for 12 h, then concentrated *in vacuo* to afford a brown powder. The powder was triturated in benzene and filtered to afford a brown solution. Crystalline material was obtained by vapor diffusion of Et_2O into this benzene solution (20 mg, 30%). Recrystallization of this material from vapor diffusion of Et_2O into a CH_2Cl_2 solution gave crystals amenable to X-ray diffraction studies.

4.3.2 Method B from 3 and PhIO:

In the glovebox, **3** (1.55 g, 1.2 mmol) was dissolved in CH_2Cl_2 (100 mL). PhIO (524 mg, 2.4 mmol) was added as a suspension in CH_2Cl_2. The solution was magnetically stirred for 5 hours and concentrated *in vacuo*. The resulting brown powder was triturated in benzene (50 ml) for 1 hour then filtered through Celite, giving a red-brown solution and brown solid. The brown solid was scraped into a flask and triturated in benzene again. This mixture was filtered through Celite, and the process repeated until no color was seen in the filtered solution. The brown solid was discarded, and the red-brown solution was concentrated *in vacuo*. Benzene was added to this solid (15 mL) to give a red-brown solution and 250 mL of Et_2O was added to afford a red-brown precipitate 2 (770 mg, 50%), collected by filtration and rinsed with Et_2O to remove iodobenzene.

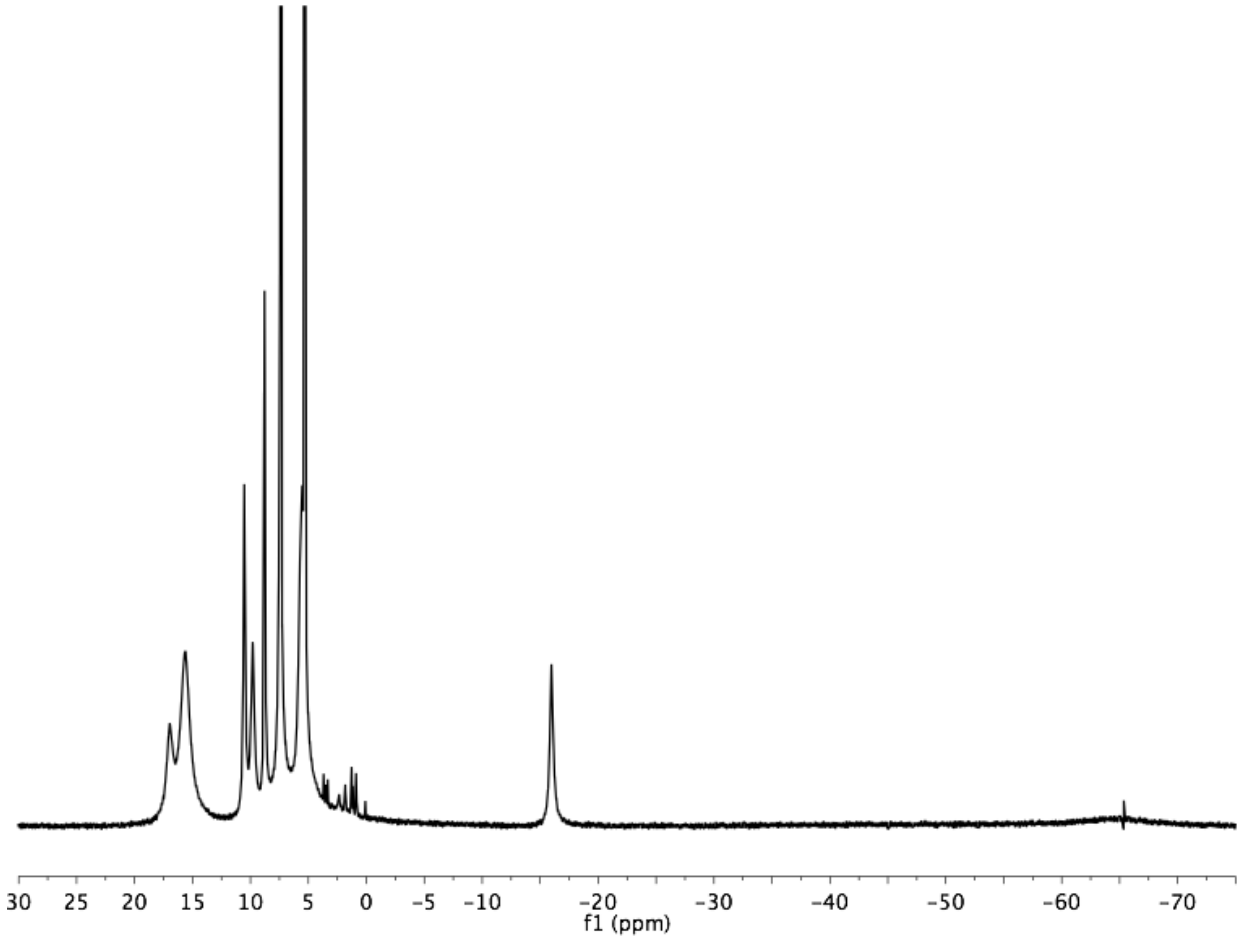

Figure S6: ^{1}H NMR spectrum of **2** in CD_2Cl_2 at 25 °C.

4.3.3 Method C from 3 and NR_4OH (R = Me, Et) and $FcPF_6$:

Under an anaerobic atmosphere, **3** (18.0 mg, 0.014 mmol) was dissolved in THF (7 mL). In a separate flask, a 35 wt. % solution of NEt_4OH in H_2O (11.6 mg, 0.028 mmol) was diluted with CH_3CN (1 mL). In a third flask, $FcPF_6$ (18.3 mg, 0.055 mmol) was dissolved in CH_3CN (1 mL). While stirring the solution of **3**, the NEt_4OH solution was added by pipette followed quickly by addition of the $FcPF_6$ solution. The red-orange solution turns green-brown upon addition of the $FcPF_6$. Volatiles were removed in vacuo after 40 minutes of stirring. The resulting green-brown solid was triturated in Et_2O and filtered to remove ferrocene. The solid was then rinsed with benzene to afford a red-orange solution of **2** and blue solid (excess $FcPF_6$). The solution was concentrated *in vacuo* to afford the red-orange powder **2** (13 mg, 70%, ca. 90% pure by ^{1}H NMR). Method B afforded the purest **2**: ^{1}H NMR (300 MHz, C_6D_6, 25 °C), 17.0, 15.6 (overlapping), 10.5 ($\Delta\nu_{1/2}$ = 50 Hz), 9.8 ($Delta\nu_{1/2}$ = 100 Hz), 8.8 ($\Delta\nu_{1/2}$ = 30 Hz), 7.5 ($\Delta\nu_{1/2}$ = 60 Hz), 5.5 ($\Delta\nu_{1/2}$ = 190),-16.0 ($\Delta\nu_{1/2}$ = 110) -64.6 ($\Delta\nu_{1/2}$ = 2400) ppm. UV-Vis (λ_{max} [ϵ (M^{-1} cm^{-1})]): 238 (1.0×10^5), 243 (1.1×10^5), 248 (1.3×10^5), 254 (1.4×10^5), 260 (1.1×10^5), 714 (200), nm. Anal. Calcd. for $C_{63}H_{48}Mn_4N_6O_13$: C, 57.46; H 3.67; N, 6.38. Found: C, 56.66; H, 3.70; N, 6.10. HRMS (TOF- MS): calcd. for $C_{63}H_{49}Mn_4N_6O_{13}$ (M+H): 1317.0879; found: 1317.0850.

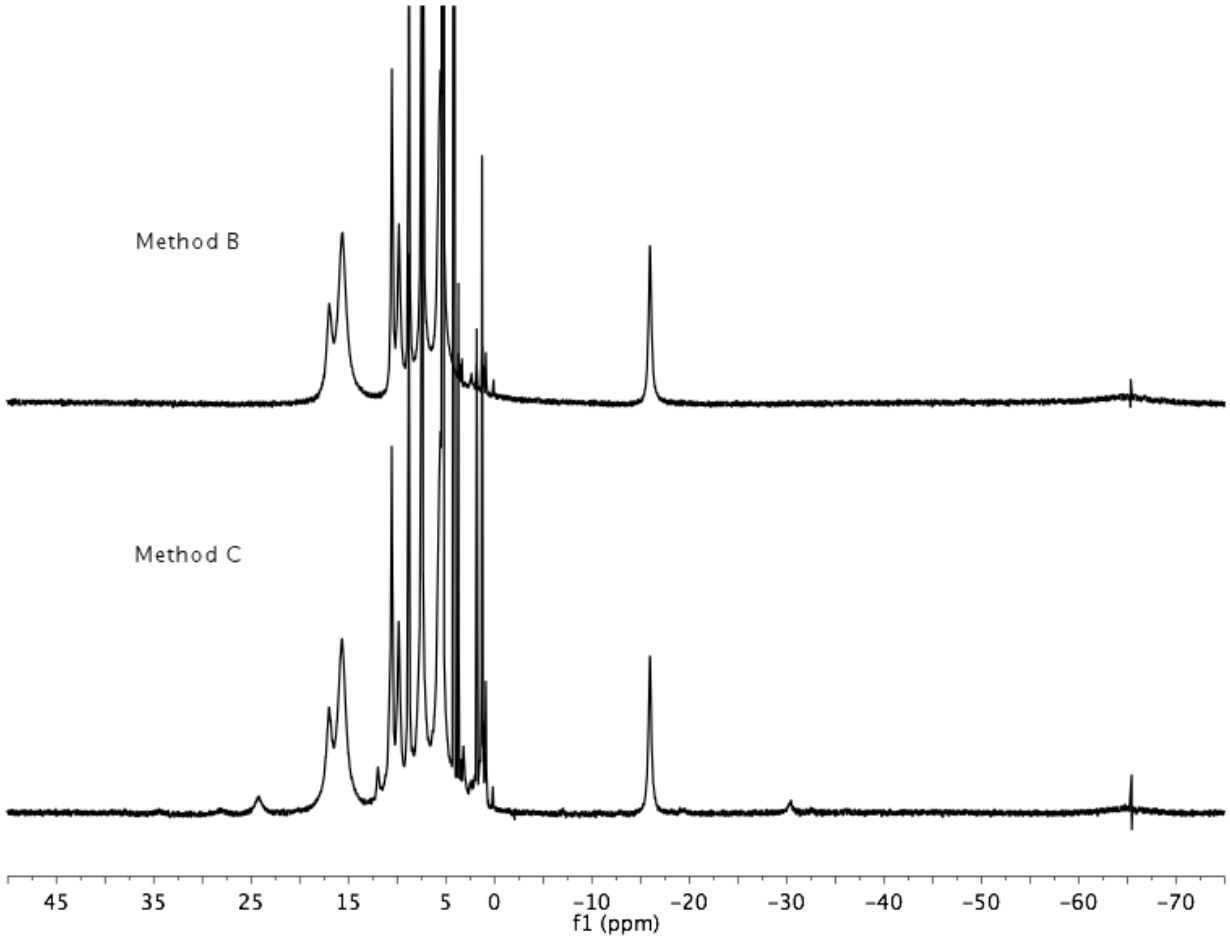

Figure S7: ^{1}H NMR spectrum of **2** synthesized from Methods B and C in CD_2Cl_2 at 25 °C.

4.4 Synthesis of $LMn^{III}_4O_3(OAc)_3$ (3).

4.4.1 Method A from 1:

In the glovebox, yellow solid **1**·THF (3.7 g, 2.9 mmol) was suspended in THF (200 mL) and $Mn(OTf)_2CH_3CN$ (1.15 g, 2.9 mmol) was separately dissolved in THF (90 mL). The solution of $Mn(OTf)_2$ was added by pipette to the solution of $LMn_3(OAc)_3$. After stirring for 20 minutes, KO_2 (0.52 g, 7.3 mmol) was added as a solid. The solution was magnetically stirred for 20 hours and then concentrated *in vacuo* to afford a brown solid. This brown solid was triturated in benzene (100 mL) for 3 hours and then filtered through Celite to afford an orange-red-brown solution. Volatiles were removed *in vacuo*, affording a red-orange powder **3** (1.7 g, 45%).

4.4.2 Method B from 2 and PMe_3:

In the glovebox, red-brown solid **2** (95.6 mg, 0.07 mmol) was dissolved in benzene (15 mL) to give a brown-red solution. PMe_3 as a 1.0M solution in THF (0.62 mL, 0.7 mmol) was added to the stirring solution. The solution was stirred for 14 hours, and volatiles were removed *in vacuo*. The resulting red-orange powder was triturated in Et_2O, collected on Celite, and rinsed with copious Et_2O to remove Me_3PO. The solid was rinsed through

the Celite with benzene and volatiles were removed *in vacuo* to afford a red-orange powder **3** (88 mg, 93%). Recrystallization from vapor diffusion of hexane into a tetrahydrofuran solution gave crystals amenable to X- ray diffraction studies. ^{1}H NMR (300 MHz, C_6D_6, 25 °C) 22.4 ($\Delta\nu_{1/2}$ = 160), 14.3 ($\Delta\nu_{1/2}$ = 60), 10.1 ($\Delta\nu_{1/2}$ = 30), 8.9 ($\Delta\nu_{1/2}$ = 30 Hz), 8.7 ($\Delta\nu_{1/2}$ = 90 Hz), 7.6 ($\Delta\nu_{1/2}$ = 100 Hz), 6.6 ($\Delta\nu_{1/2}$ = 60 Hz), 5.3 ($\Delta\nu_{1/2}$ = 20 Hz), -12.9 ($\Delta\nu_{1/2}$ = 50 Hz), - 46.0 ($\Delta\nu_{1/2}$ = 1000 Hz) ppm. UV-Vis (λ_{max} [ϵ (M^{-1} cm^{-1})]): 234 (7.0×10^4), 239 (6.9×10^4), 244 (6.6×10^4), 249 (6.0×10^4), 256 (5.3×10^4), 262 (4.7×10^4), 396 (2170), 497 (980) nm. Anal. Calcd. for $C_{67}H_{56}Mn_4N_6O_{13}$ (**LMn$^{III}_4$O$_3$(OAc)$_3$·THF**): C, 58.61; H, 4.11; N, 6.12. Found: C, 58.94; H, 4.00; N, 6.24. An X-ray diffraction study of a single crystal of **LMn$^{III}_4$O$_3$(OAc)$_3$** showed that the compound crystallizes with four THF molecules.

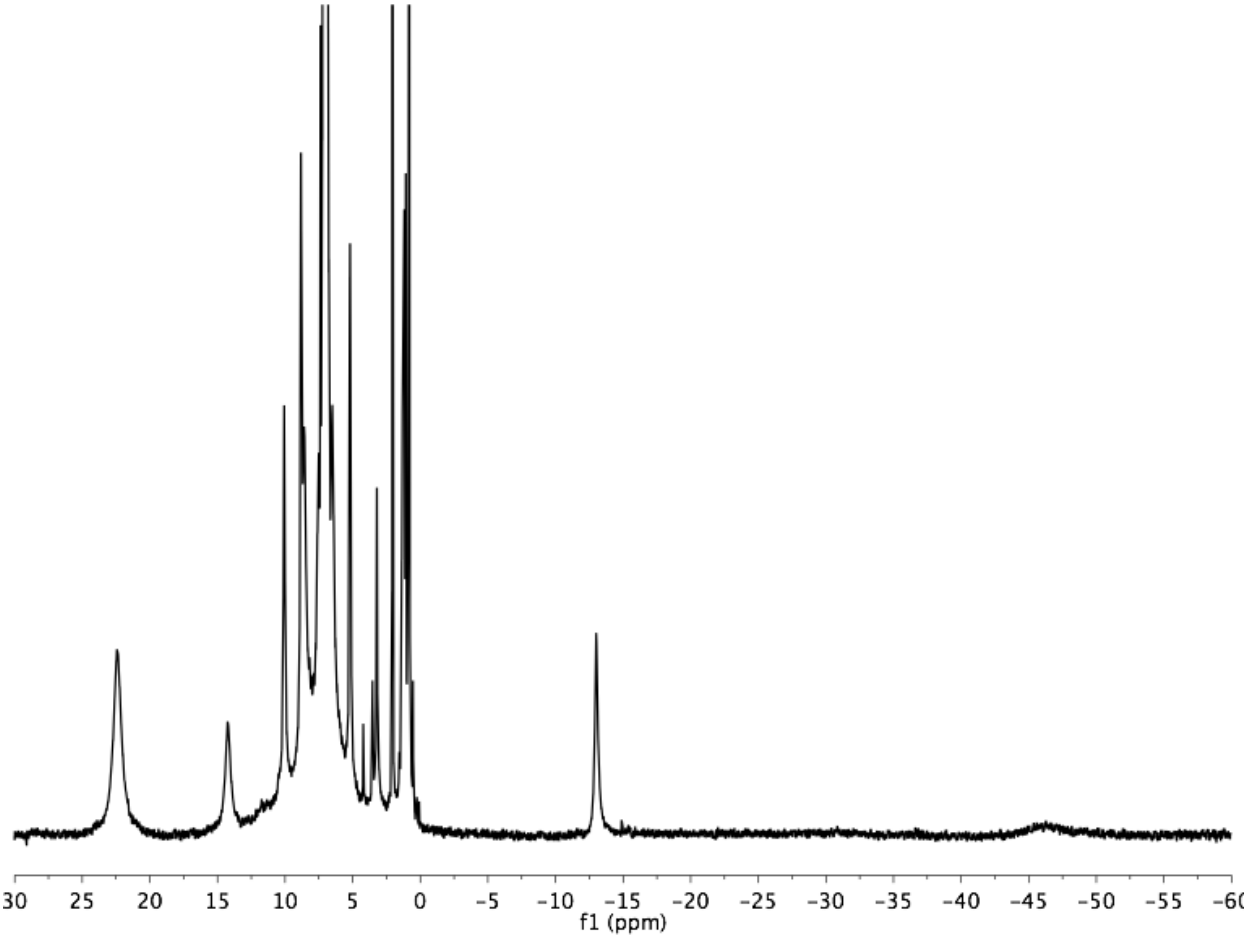

Figure S8: ^{1}H NMR spectrum of **3** in C_6D_6 at 25 °C.

4.5 Synthesis of LMn$^{IV}_3$CaO$_4$(OAc)$_3$·THF (4).

Improving upon the published procedure, [15] in the glovebox, a roundbottom flask equipped with a stir bar was charged with **1** (1.00 g, 0.835 mmol) and Ca(OTf)$_2$ (0.310 g, 0.917 mmol, 1.1 equiv). THF (130 mL) was added, and the yellow heterogeneous mixture was stirred at room temperature for 5 min. KO_2 (0.178 g, 2.50 mmol, 3

equiv) was added to the mixture as a solid, and the mixture was stirred at room temperature for 12 h, darkening to red-brown. The mixture was filtered through Celite, then concentrated *in vacuo* to yield a red-brown solid. The solid was washed with benzene (50 mL) and acetonitrile (100 mL), then extracted with THF. The THF extract was concentrated *in vacuo* to yield the product as a red solid (0.053 g, 5 %). The product was characterized via cyclic voltammetry and ESI-MS, and spectral features math those of the previously published procedure.

4.6 Synthesis of $LMn^{IV}_3ScO_4(OAc)_3(OTf)$ (5).

In the glovebox, a scintillation vial equipped with a stir bar was charged with **4** (0.101 g, 0.073 mmol) and $Sc(OTf)_3$ (0.036 g, 0.073 mmol, 1.0 equiv). DMF (3 mL) was added, and the dark red-brown solution was stirred at room temperature for 5 min. Diethyl ether (35 mL) was added to precipitate a dark red-brown solid. The precipitate was collected by filtration, then recrystallized from acetonitrile/diethyl ether to afford the product as a dark brown crystals (0.069 g, 65 %). ^{1}H NMR (CD_2Cl_2, 300 MHz): δ 12.1, 11.8, 9.5, 8.0, 6.2, 4.4, -1.1, -23.8 ppm. ^{19}F NMR (CD_2Cl_2): δ -77.5 ppm. UV-Vis (CH_2Cl_2, λ_{max} [ϵ (M^{-1} cm^{-1})]): 243 (6.6×10^4), 350 (shoulder, 1.2×10^4). Anal. Calcd. for $C_64H_48F_3Mn_3N_6O_16SSc$: C, 52.80; H, 3.32; N, 5.77. Found: C, 53.07; H, 3.41; N, 5.65.

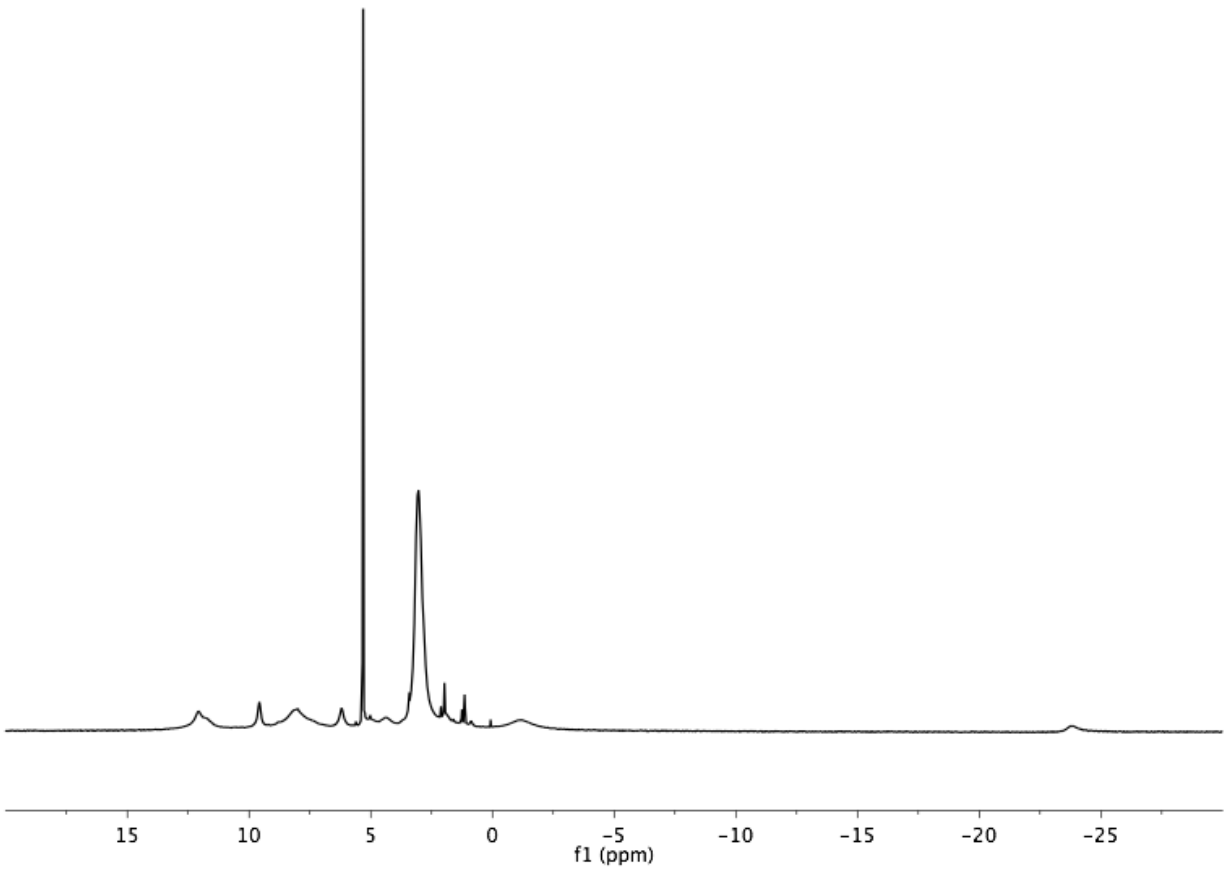

Figure S9: ^{1}H NMR spectrum of **5** in CD_2Cl_2 at 25 °C.

5 Reactivity comparison of 2 and 4 and 5 with PMe_3

In the glovebox, **2** (0.0091 g, 0.0069 mmol), **4** (0.0095 g, 0.0069 mmol), and **5** (0.0079 g, 0.0054 mmol) respectively, were dissolved in 0.8 mL (0.7 mL for **5**) of a DMF solution of $[PPh_4][BF_4]$ (3.4 mg, 0.0079 mmol, 1.14 equiv for **2** and **4**; 2.3 mg, 0.0054 mmol, 1.0 equiv for **5**) and transferred to separate J. Young NMR tubes (PPh_4^+ serves as an internal standard). A solution of PMe_3 (18 μL, 0.78 M in THF, 0.014 mmol, 2.0 equiv for **2** and **4**; 20 μL, 0.78 M in THF, 0.015 mmol, 2.9 equiv for **5**) was added via syringe to both mixtures, and the tubes were sealed with Teflon caps. The reactions were monitored using ^{31}P NMR spectroscopy referenced to an external standard of 85% H_3PO_4.

Within 15 min. at RT, ^{31}P NMR spectroscopy of the reaction with **2** indicates consumption of one equivalent of PMe_3 as well as a broadened PMe_3 signal (Figure S10). No signal corresponding to $OPMe_3$ is observed. ^{31}P NMR spectroscopy of the solutions of **4** and **5** show no consumption of PMe3 (Figure S10). No changes in the ^{31}P NMR spectra of the mixtures containing **2** and **4** are observed after 18 h at RT (Figure S11). Approximately one equivalent of PMe_3 has been consumed in the reaction containing **5**, though no $OPMe_3$ is detected by GC-MS, likely indicating an alternate decomposition route not involving oxygen-atom transfer.

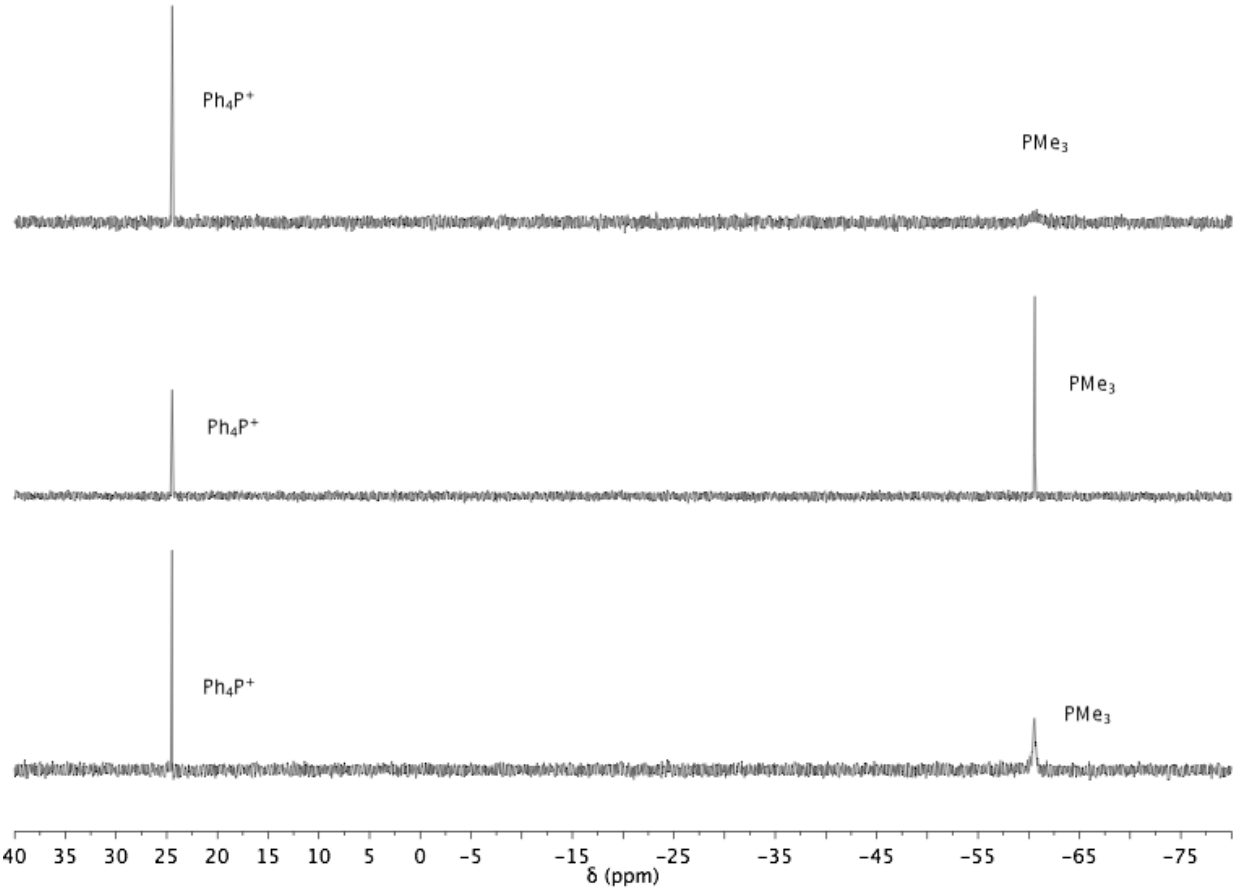

Figure S10: ^{31}P NMR spectra of the reaction of **2** and PMe_3 (top), **4** and PMe_3 (middle), and **5** and PMe_3 (bottom) in DMF after 15 min. at RT. $[PPh_4][BF_4]$ (1 equiv) is present as an internal standard

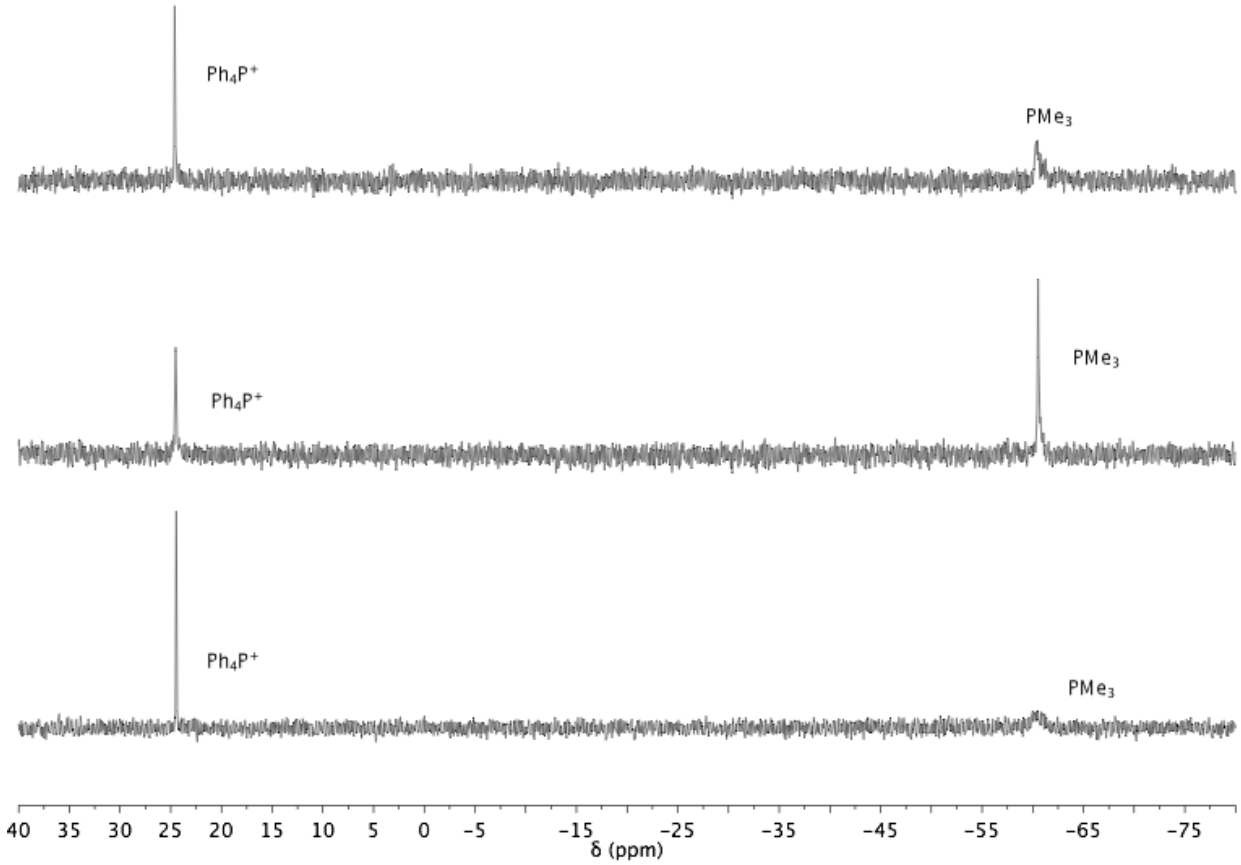

Figure S11: ^{31}P NMR spectra of the reaction of **2** and PMe_3 (top), **4** and PMe_3 (middle), and **5** and PMe_3 (bottom) in DMF after 18 hours at RT. $[PPh_4][BF_4]$ (1 equiv) is present as an internal standard

6 Cyclic Voltammetry

Electrochemical measurements were recorded under a nitrogen atmosphere in an MBraun glovebox at 25 °C with a Pine Instrument Company AFCBP1 bipotentiostat. An auxiliary Pt-coil electrode, a Ag/Ag^+ reference electrode (0.01 M $AgNO_3$ in CH_3CN), and a 3.0 mm glassy carbon electrode disc (BASI) were used. Data were recorded using the Pine Instrument Company AfterMath software package. All reported values were referenced to an internal ferrocene/ferrocenium couple. The electrolyte solutions were 0.1 M nBu$_4$NPF$_6$ in DMF, dimethylacetamide (DMA) or THF.

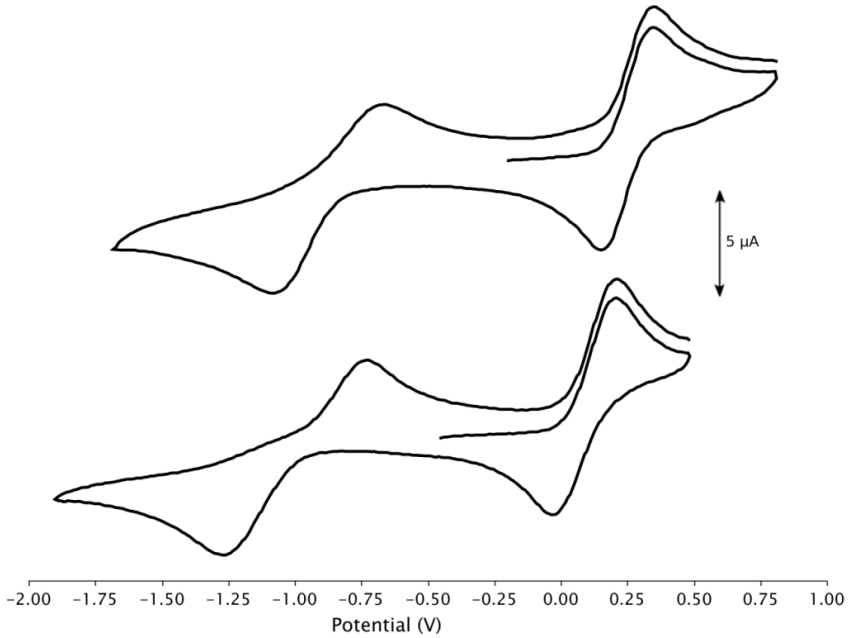

Figure S12: Cyclic voltammograms of **2** (top) and **3** (bottom). The scan rate was 50 mV/s in the positive direction at an analyte concentration of 1.0 mM and electrolyte of 0.1M $n\mathrm{Bu_4NPF_6}$ in THF. Open-circuit potential (vs $\mathrm{FeCp_2/FeCp_2^+}$) for **2** = -200 mV and for **3** = -460 mV. $\mathrm{E_{1/2}}$ values: $\mathbf{3^+/3}$ = +0.10 V; $\mathbf{3/3^-}$ = -1.0 V; $\mathbf{2^+/2}$ = +0.25 V; $2/2^-$ = -0.87 V.

7 Magnetism Studies

7.1 General Considerations

DC magnetic susceptibility measurements were carried out in the Molecular Materials Research Center in the Beckman Institute of the California Institute of Technology on a Quantum Design MPMS instrument running MPMS MultiVu software. Powdered samples (0.040–0.059 g) were fixed in eicosane (0.10–0.12 g) in gelatin capsules or in plastic wrap and suspended in clear plastic straws. Data were recorded at 0.5 T from 4–300 K. Diamagnetic corrections were made using the average experimental magnetic susceptibility of $\mathbf{H_3L}$ at 0.5 T from 100–300 K (-593 $\times$ 10^{-6} $\mathrm{cm^3/mol}$) in addition to the values of Pascal's constants for amounts of solvent quantified for each sample using elemental analysis.

7.2 Discussion

Plots of the $\chi_M T$ data taken at 0.5 T are shown in Fig. S13. For **2**, the $\chi_M T$ value decreases to 0.8 $\mathrm{cm^3\ mol^{-1}}$ K at 4 K and approaches a value of 6 $\mathrm{cm^3\ mol^{-1}}$ K at 300 K, indicating antiferromagnetic coupling between the manganese centers. The room temperature $\chi_M T$ value of 6 $\mathrm{cm^3\ mol^{-1}}$ K for complex **2** is lower than the expected spin-only value (9.8 $\mathrm{cm^3\ mol^{-1}}$ K, $g = 2$) of two uncoupled $\mathrm{Mn^{III}}$ ions ($S = 2$) and two uncoupled $\mathrm{Mn^{IV}}$ ions ($S = 3/2$). Antiferromagnetically coupled manganese clusters in the literature have also shown significant deviation at 300 K from the expected spin-only value. [16–20]

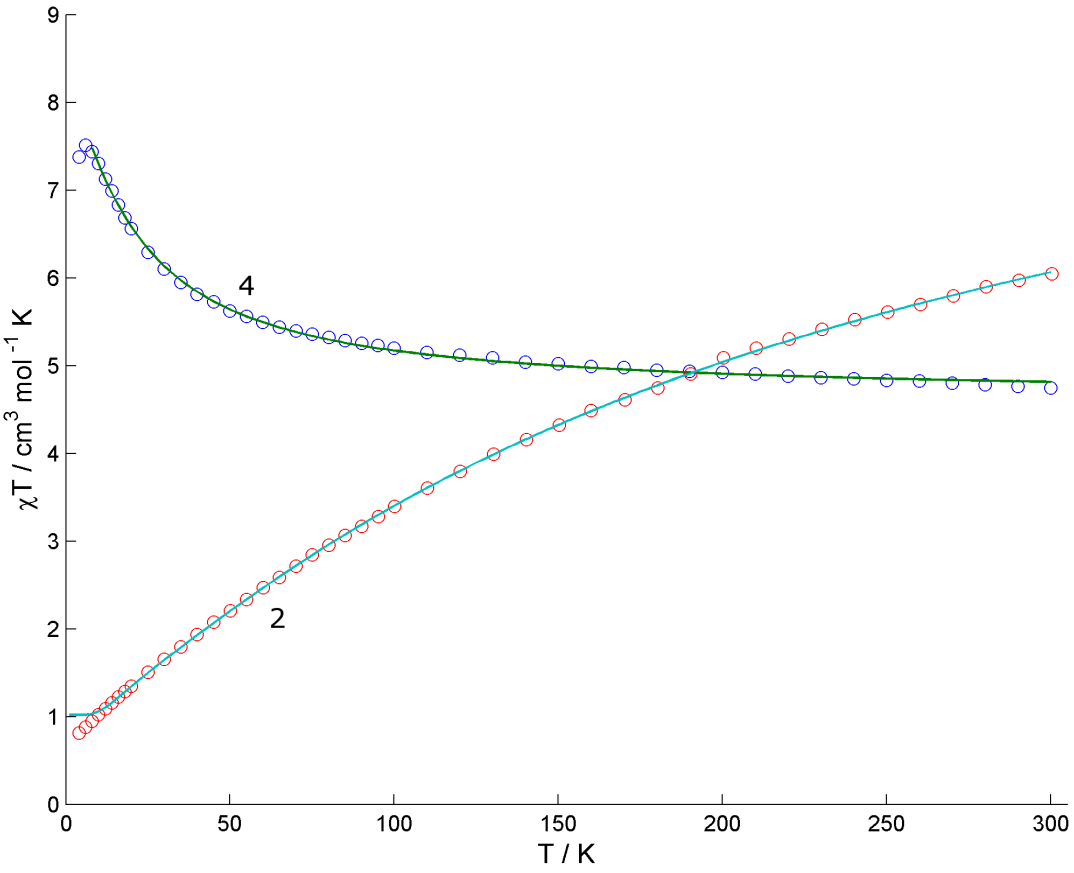

Figure S13: $\chi_M T$ vs. T data (circles) and fits (lines) for compounds **2** and **4**. See Table S7 for fit parameters.

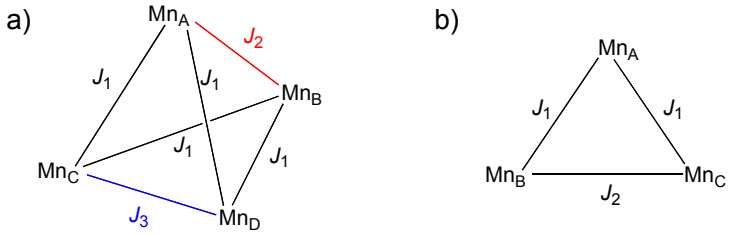

Figure S14: Exchange coupling models employed for (a) **2** and (b) **4**. For compound **2**, the spins used were $S =$ 2, 2, 3/2, and 3/2 for Mn_A, Mn_B, Mn_C and Mn_D, respectively. For **4**, the spins used were all $S = 3/2$.

Table S7: Magnetic susceptibility fitting parameters.

Compound	Diamagnetic Correction ($\times 10^{-6}$ cm^3/mol)	J_1 (cm^{-1})	J_2 (cm^{-1})	J_3 (cm^{-1})	g	R ($\times 10^{-5}$)
$LMn^{IV}{}_2Mn^{III}{}_2O_4(OAc)_3{\cdot}0.5C_6H_6$ (**2**)	-722	-13.9	-6.3	-18.2	2.02	1.6
$LMn^{IV}{}_3CaO_4(OAc)_3{\cdot}3DMF$ (**4**)	-721	3.5	-1.8	--	1.81	2.2

The magnetic susceptibility data for **2** were fit to the magnetic susceptibility equation derived from the isotropic spin Hamiltonian for three coupling constants, J_1, J_2, and J_3. Specifically, the manganese centers were

modeled as an asymmetric tetrahedron (Figure S14a), with the basal three manganese centers (Mn_B, Mn_C and Mn_D) modeled as an isosceles triangle. The exchange pathways between the apical Mn^{III} center (Mn_A) and the two Mn^{IV} centers (Mn_C, Mn_D), J_1, were assumed to be the same as the interactions between the Mn^{IV} centers and the basal Mn^{III} (Mn_B) in order to allow the eigenvalues to be determined for the isotropic spin Hamiltonian [Eq. (3)]. The interactions between the Mn^{III} centers and the interactions between the two Mn^{IV} centers were modeled as separate parameters (J_2 and J_3, respectively).

$$\widehat{H} = -2J_1[(\widehat{S}_A \cdot \widehat{S}_C) + (\widehat{S}_A \cdot \widehat{S}_D) + (\widehat{S}_B \cdot \widehat{S}_C) + (\widehat{S}_B \cdot \widehat{S}_D)] - 2J_2(\widehat{S}_A \cdot \widehat{S}_B) - 2J_3(\widehat{S}_C \cdot \widehat{S}_D) \quad (3)$$

The eigenvalues were determined using the Kambe method. [21] The data were fit from 10–300 K using Matlab [22] by minimizing $R = \sum |(\chi_M T)_{\mathrm{obs}} - (\chi_M T)_{\mathrm{calc}}|^2 / \sum (\chi_M T)^2_{\mathrm{obs}}$ (Table S7). For **2**, the J values are negative, indicating antiferromagnetic interactions between the manganese centers as expected. The J values for all coupling pathways are relatively small (<25 cm^{-1}, ca. 0.07 kcal/mol), *consistent with the values found by QM (see main text).*

For **4**, dominant ferromagnetic coupling between Mn ions is observed (Figure S13); at 6 K, the $\chi_M T$ value increases to a maximum of 7.5 cm^3 mol^{-1} K, which is slightly lower than the expected spin-only value of a $S = 9/2$ system (10.0 cm^3 mol^{-1} K, $g = 1.8$), but greater than the expected spin-only value of a $S = 7/2$ system (6.4 cm^3 mol^{-1} K, $g = 1.8$). The $\chi_M T$ value decreases from the maximum below 6 K, likely due to low temperature effects such as intermolecular exchange interactions. At 300 K, the $\chi_M T$ value approaches 4.7 cm^3 mol^{-1} K, which is close to the expected spin-only value of three uncoupled Mn^{IV} ions ($S = 3/2$, 1.5 cm^3 mol^{-1} K, $g = 1.8$).

The $\chi_M T$ data taken at 0.5 T of **4** were fit to the magnetic susceptibility equation derived from the isotropic spin Hamiltonian for two coupling constants, J_1 and J_2 [Eq. (4)], where the exchange pathways between the three Mn^{IV} centers are modeled as an isosceles triangle (Figure S14b). The eigenvalues were determined (*vide supra*) and the data were fit from 10–300 K using Matlab [22] by minimizing $R = \sum |(\chi_M T)_{\mathrm{obs}} - (\chi_M T)_{\mathrm{calc}}|^2 / \sum (\chi_M T)^2_{\mathrm{obs}}$ (Table S7) to give J_1 = 3.5 cm^{-1} and J_2 = -1.8 cm^{-1}. The larger absolute value of J_1 leads to the dominant ferromagnetic interactions observed in the low temperature susceptibility data, but the relatively weak coupling observed may lead to population of higher energy lower spin states even at low temperatures. A related [$Ca_2Mn^{IV}{}_3O_4$] cluster prepared by Christou and co-workers showed similar exchange interactions, with J_1 = 40.5 cm^{-1} and J_2 = -10.8 cm^{-1}. [23] The stronger coupling observed between the Mn^{IV} centers of the latter complex may be due to the more acute Mn-O-Mn angles [92.11(11)-96.81(12)°] compared to the greater Mn-O-Mn angles [95.09(9) -100.25(10)°] of complex **4**, since exchange interactions are known to be greatly affected by angle changes. [23]

$$\widehat{H} = -2J_1[(\widehat{S}_A \cdot \widehat{S}_B) + (\widehat{S}_A \cdot \widehat{S}_C)] - 2J_2(\widehat{S}_B \cdot \widehat{S}_C) \quad (4)$$

8 ^{18}O Labeling Studies

8.1 ESI-MS Procedures

In a nitrogen glovebox, samples were dissolved in anhydrous, degassed CH_2Cl_2 and diluted to $\approx$ 10 μM in M.S. vials. These vials were then transferred to 20 mL vials that were then capped and taped shut with electrical tape. Separately, a small sample of anhydrous, degassed CH_2Cl_2 in a 4 mL vial was capped and taped. These were removed from the glovebox and taken immediately to the instrument. After rinsing the line and inlet with wet, aerobic CH_2Cl_2, the line was rinsed quickly with the anhydrous, degassed CH_2Cl_2 followed immediately by the sample. The spectra shown are averages of $\geq$70 scans.

Synthetic/Control Procedures:

*All experiments performed in duplicate or greater.

*Mass spectra corresponding to each experiment are included directly below said experiment.

8.2 Enrichment of NR_4OH with ^{18}O.

In an anaerobic, water-containing glovebox, the desired amount (generally <10μmol) of $NMe_4OH{\cdot}5H_2O$ (solid) or 35 wt. % NEt_4OH in H_2O (solution) was weighed out. For NEt_4OH, excess H_2O was removed first *in vacuo*. Ca. 10 μL 97% $H_2{}^{18}O$ was added, full dissolution of the white solid was observed, and then volatiles were removed *in vacuo*. This procedure was repeated a total of three times to afford ca. 96% 18-labelled $NR_4{}^{18}OH$.

8.3 Synthesis of $LMn^{III}{}_2Mn^{IV}{}_2{}^{16}O_3{}^{18}O(OAc)_3$ (2*).

In an anaerobic, water-containing glovebox, **3** (3.8 mg, 0.003 mmol) was dissolved in THF (1.2 mL). In a separate flask, $NMe_4OH{\cdot}5H_2O$ (1.1 mg, 0.006 mmol) was enriched with ^{18}O by the method above. $H_2{}^{18}O$ (1.1μL, 0.060 mmol) was added to the $NMe_4{}^{18}OH$, followed by CH_3CN (0.07 mL) and THF (0.2 mL). In a third flask, $FcPF_6$ (3.9 mg, 0.012 mmol) was dissolved in CH_3CN (0.07 mL) and THF (0.2 mL). While stirring the solution of $NMe_4{}^{18}OH$ and $H_2{}^{18}O$, the solution of **3** was added by syringe, followed by a rinse of the syringe with THF (0.2 mL). One minute after addition of **3**, the $FcPF_6$ solution was added, and the syringe was again rinsed with THF (0.2 mL) and CH_3CN (0.06 mL). The final concentration is 1.33mM in 10:1 THF/CH_3CN. The red-orange solution turns green-brown upon addition of the dark blue $FcPF_6$. Volatiles were removed *in vacuo* after 35 minutes of stirring. The resulting green-brown solid was triturated in Et_2O and filtered to remove ferrocene. The solid was then rinsed with benzene to afford a red-orange solution of **2*** and blue solid (excess $FcPF_6$). The solution was concentrated *in vacuo* to afford the red-orange powder **2***.

8.4 Synthesis of $LMn^{III}{}_4{}^{16}O_2{}^{18}O(OAc)_3$ (3*).

See Method B in the synthesis of **3**.

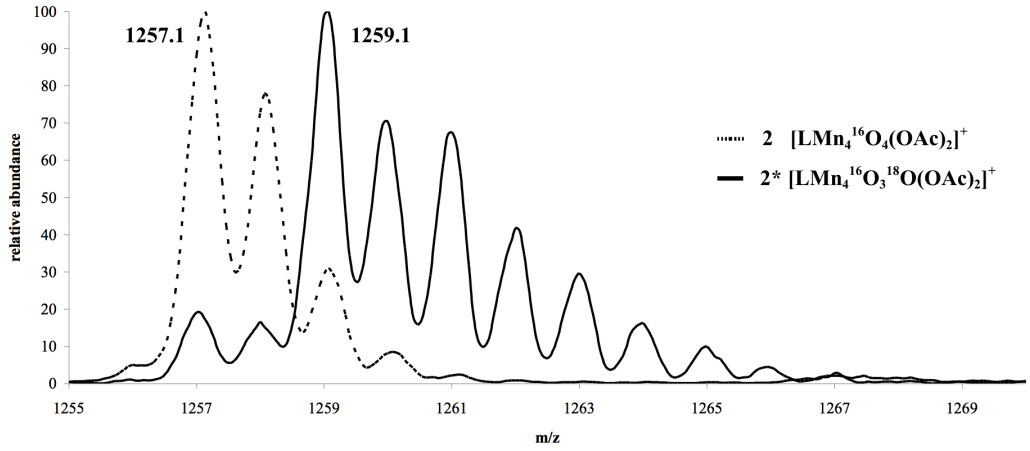

Figure S15: Electrospray Ionization Mass Spectra of compound **2** (solid line) isolated from the labeling experiments and natural abundance compound **2** (dashed line). The 1257.1 and 1259.1 peaks correspond to the unlabeled and labeled mass with one acetate lost from the parent ion - $LMn_4O_4(OAc)_2^+$. Conditions: **3** (1 equiv.), $NMe_4{}^{18}OH$ (2 equiv.), $H_2{}^{18}O$ (ca. 20 equiv.), $FcPF_6$ (4 equiv.), 10:1 THF/CH_3CN, RT, 35 minutes.

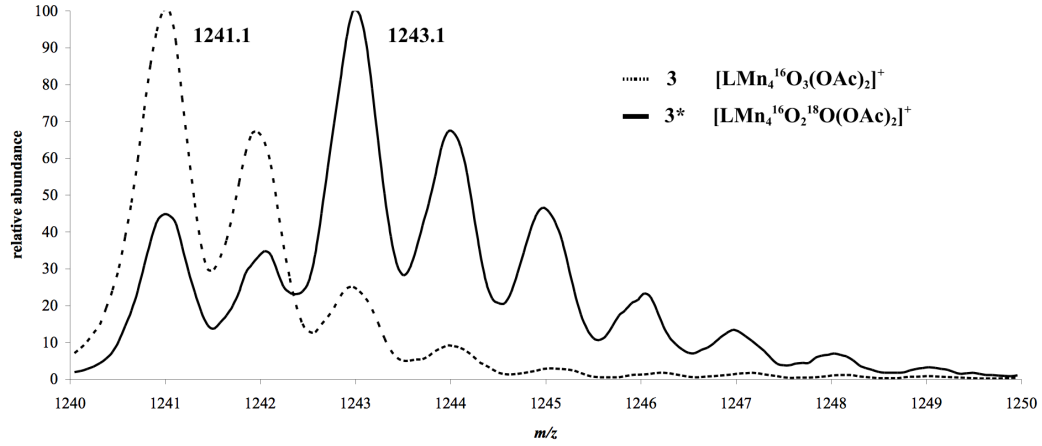

Figure S16: Electrospray Ionization Mass Spectra of natural abundance **3** (dashed lines) isolated from the reaction of unlabeled **2** and compound **3*** (solid line) isolated from the reaction of labeled **2*** with PMe_3. The 1241.1 and 1243.1 peaks correspond to the unlabeled and labeled mass with one acetate lost from the parent ion - $LMn_4O_3(OAc)_2^+$. Reaction Conditions: **2*** (1 equiv.), PMe_3 (10 equiv.), C_6H_6, RT, 24 hrs.

8.5 2 + $H_2{}^{18}O$ Control.

In an anaerobic, water-containing glovebox, **2** (4 mg, 0.003 mmol) was dissolved in 10:1 THF/CH_3CN (2.3 mL) to give a 1.33 mM solution (the concentration used in the water incorporation experiments). $H_2{}^{18}O$ (1.1 μL, 0.060 mmol) was added by syringe and the solution was stirred for 35 minutes (the time course of the water incorporation experiments). Volatiles were removed *in vacuo*. The resulting solid was rinsed with dry Et_2O and rinsed through with C_6H_6 and concentrated *in vacuo*.

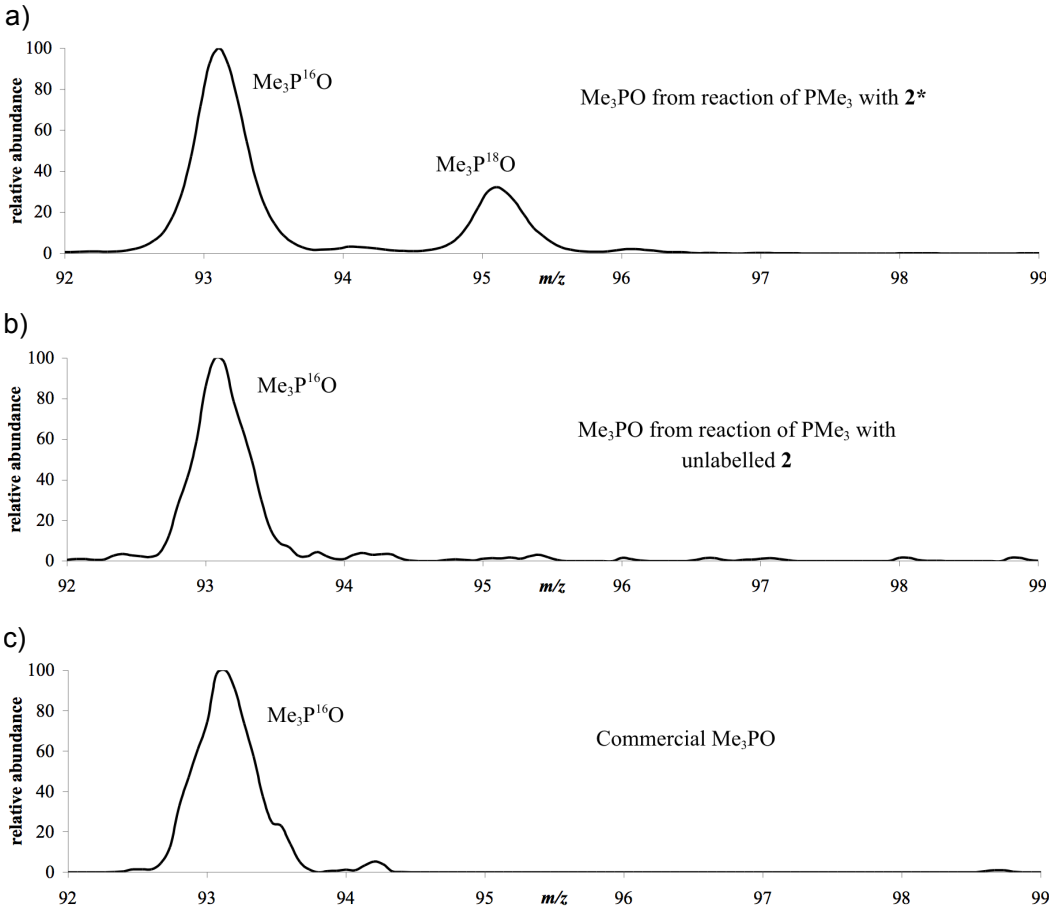

Figure S17: Electrospray Ionization Mass Spectra of a) trimethylphosphine oxide isolated from the reaction of PMe_3 with **2***, b) trimethylphosphine oxide isolated from the reaction of PMe_3 with unlabeled **2**, and c) commercial trimethylphosphine oxide (Alfa Aesar)

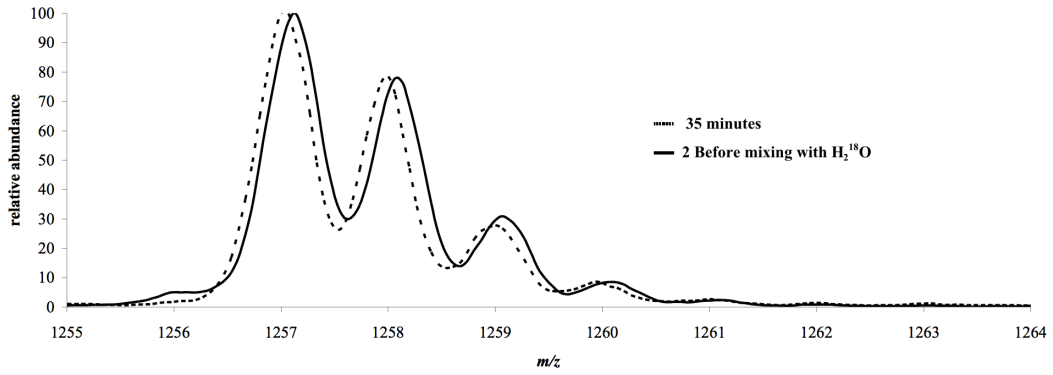

Figure S18: Electrospray Ionization Mass Spectra of natural abundance **2** (solid line) and compound **2** (dashed line) after stirring for 35 minutes in the presence of $H_2{}^{18}O$. Conditions: **2** (1 equiv.), $H_2{}^{18}O$ (20 equiv.), 10:1 THF/CH3CN, 35 minutes, RT.

8.6 3 + $H_2{}^{18}O$ Control.

In an anaerobic, water-containing glovebox, **3** (3.9 mg, 0.003 mmol) was dissolved in 10:1 THF/CH_3CN (2.3 mL) to give a 1.33 mM solution. $H_2{}^{18}O$ (1.1 μL, 0.060 mmol) was added by syringe and the solution was stirred for

35 minutes. Volatiles were removed *in vacuo*. The resulting solid was rinsed with dry Et_2O and rinsed through with C_6H_6 and concentrated *in vacuo*.

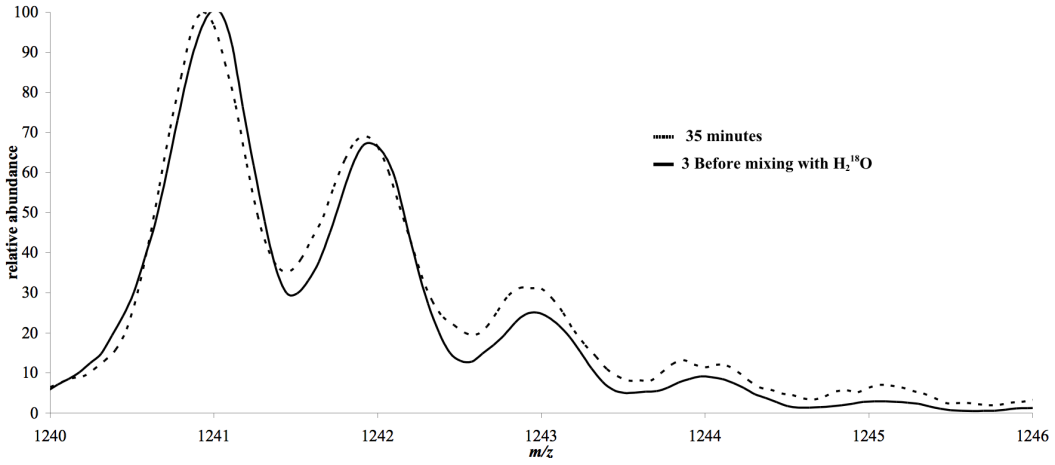

Figure S19: Electrospray Ionization Mass Spectra of natural abundance **3** (solid lines) and compound **3** (dashed lines) after stirring for 35 minutes in the presence of $H^{218}O$. Conditions: **3** (1 equiv.), $H^{218}O$ (20 equiv.), 10:1 THF/CH_3CN, 35 minutes, RT.

8.7 2 + $H_2{}^{18}O$ + $FcPF_6$ Control.

In an anaerobic, water-containing glovebox, **2** (3.8 mg, 0.003 mmol) was dissolved in THF (1.6 mL). In a second flask, $FcPF_6$ (3.8 mg, 0.012 mmol) was dissolved in CH_3CN (0.10 mL) and THF (0.2 mL). $H_2{}^{18}O$ (1.0 μL, 0.060 mmol) was added to the solution of **2**, followed one minute later by the $FcPF_6$ solution. The syringe was rinsed with THF (0.2 mL) and CH_3CN (0.10 mL). The final concentration is 1.33 mM in 10:1 THF/CH_3CN. The red-orange solution turns green-blue upon addition of the dark blue $FcPF_6$. Volatiles were removed in vacuo after 35 minutes of stirring. The resulting green-brown solid was triturated in dry Et_2O and filtered. The solid was then rinsed with benzene to afford a red-orange solution of **2** and blue solid (excess $FcPF_6$). The solution was concentrated *in vacuo* to afford a red-orange powder of **2**.

8.8 2 + $H_2{}^{18}O$ + $NMe_4{}^{18}OH$ + $FcPF_6$ Control.

In an anaerobic, water-containing glovebox, **2** (3.9 mg, 0.003 mmol) was dissolved in THF (1.3 mL). In a separate flask, $NMe_4OH{\cdot}5H_2O$ (1.1 mg, 0.006 mmol) was enriched with ^{18}O by the method above. $H_2{}^{1}8O$ (1.1μL, 0.060 mmol) was added to the $NMe_4{}^{18}OH$, followed by CH_3CN (0.07 mL) and THF (0.2 mL). In a third flask, $FcPF_6$ (3.9 mg, 0.012 mmol) was dissolved in CH_3CN (0.07 mL) and THF (0.2 mL). While stirring the solution of $NMe_4{}^{18}OH$ and $H_2{}^{18}O$, the solution of **2** was added by syringe, followed by a rinse of the syringe with THF (0.2 mL). One minute after addition of **2**, the $FcPF_6$ solution was added, and the syringe was again rinsed with THF (0.2 mL) and CH_3CN (0.07 mL). The final concentration is 1.33mM in 10:1 THF/CH_3CN. The red-orange solution turns green-brown upon addition of the dark blue $FcPF_6$. Volatiles were removed *in vacuo* after 35 minutes of stirring. The resulting green-brown solid was triturated in dry Et_2O and filtered to remove any ferrocene formed.

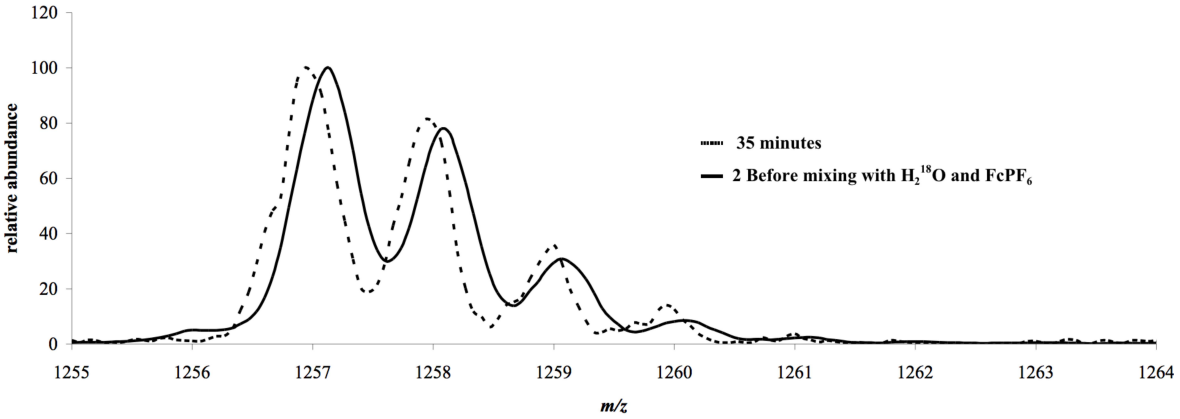

Figure S20: Electrospray Ionization Mass Spectra of natural abundance **2** (dashed lines) and compound **2** (solid lines) after stirring for 35 minutes in the presence of $H_2{}^{18}O$ and $FcPF_6$. Conditions: $H_2{}^{18}O$ (20 equiv.), $FcPF_6$ (4 equiv.), 10:1 THF/CH_3CN, 35 minutes, RT.

The solid was then rinsed with benzene to afford a red-orange solution of **2** and blue solid (excess $FcPF_6$). The solution was concentrated *in vacuo* to afford a red-orange powder of **2**.

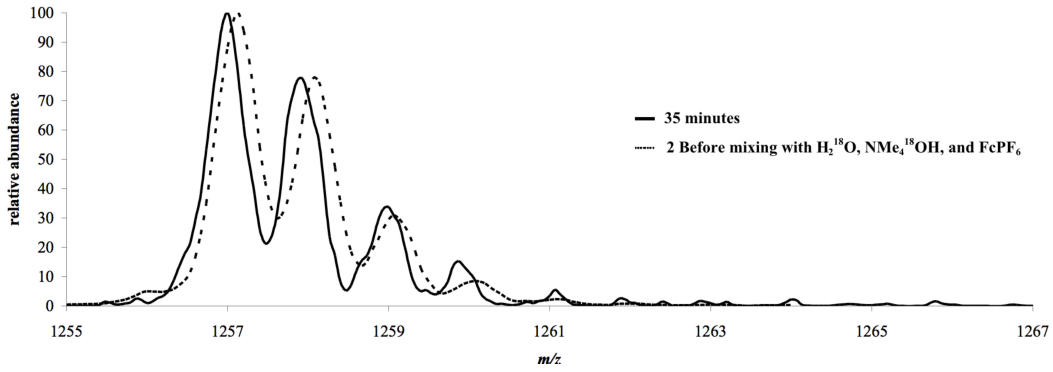

Figure S21: Electrospray Ionization Mass Spectra of natural abundance **2** (dashed lines) and compound **2** after stirring for 35 minutes (solid lines) in the presence of $H_2{}^{18}O$, $NMe_4{}^{18}OH$ and $FcPF_6$. Conditions: **2** (1 equiv.), $H_2{}^{18}O$ (20 equiv.), $NMe_4{}^{18}OH$ (2 equiv.), $FcPF_6$ (4 equiv.), 10:1 THF/CH_3CN, 35 minutes, RT.

8.9 2* + 3 + PMe_3 Control.

In a nitrogen glovebox, **2*** (1.2 mg, 9x10^{-4} mmol) was mixed with 3 (5.9 mg, 0.005 mmol) as solids. These were dissolved in C_6H_6 (2.7 mL) and PMe_3 was added (10 μL, 50 mM in THF). This solution was allowed to stir, and aliquots were taken and pumped down.

8.10 2* + 3 Control.

In a nitrogen glovebox, **2*** (1.0 mg, 0.002 mmol) and **3** (1.0 mg, 0.002 mmol) were mixed as solids. This solid mixture was then dissolved in: 10:1 THF/CH_3CN (1.2 mL to give a solution 1.33 mM in **2***+**3** (0.67 mM in each)); C_6H_6 (0.75 mL to give a solution 2 mM in **2***+**3**). Volatiles were removed in vacuo after 35 minutes. The

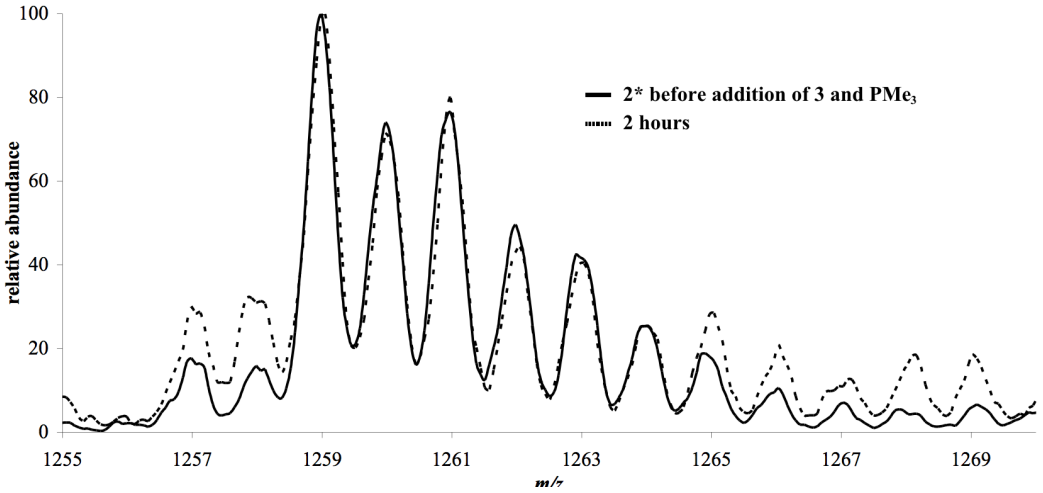

Figure S22: Electrospray Ionization Mass Spectra of **2*** before addition of **3** and PMe_3 (solid line) and two hours after addition (dashed line). Conditions: **2*** (1 equiv.), **3** (5 equiv.), PMe_3 (0.5 equiv.), C_6H_6, RT

resulting solid was rinsed with dry Et_2O and rinsed through with C_6H_6 and concentrated *in vacuo*.

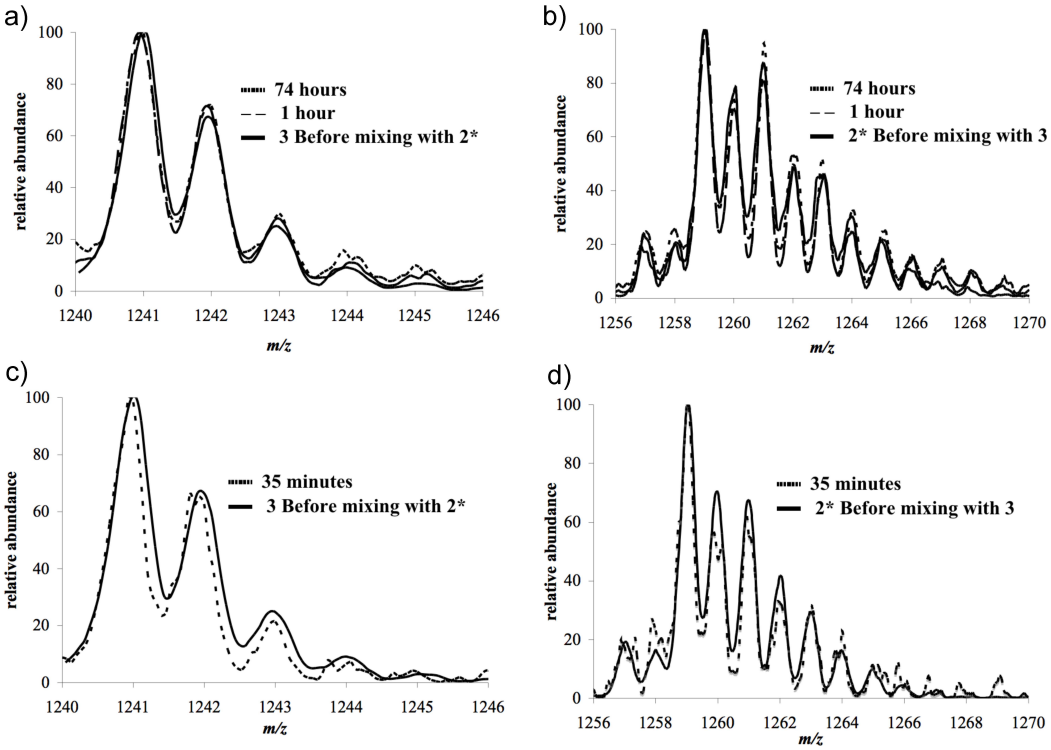

Figure S 23: Electrospray Ionization Mass Spectra of **3** and **2*** from their mixture in benzene and 10:1 THF/CH_3CN. a) Natural abundance **3** (solid line) before mixture with **2*** and 1 hour (large-dashed line) and 74 hours (short-dashed line) after mixture with **2*** in benzene. b) Labeled **2*** (solid line) before mixture with **3** and **1** hour (large-dashed line) and 74 hours (short-dashed line) after mixture with **3** in benzene. c) Natural abundance **3** (solid line) before mixture with **2*** and 35 minutes (short-dashed line) after mixture with **2*** in 10:1 THF/CH_3CN. d) Labeled **2*** (solid line) before mixture with **3** and 35 minutes (short-dashed line) after mixture with **3** in 10:1 THF/CH_3CN.

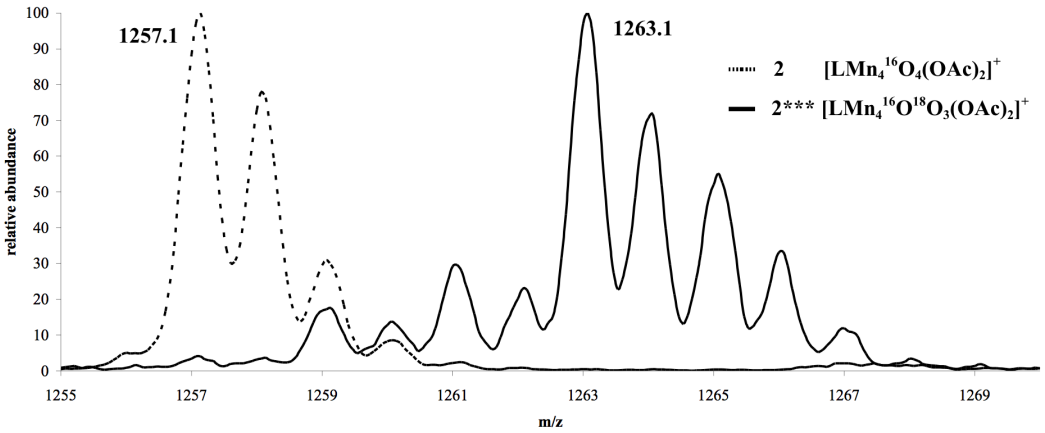

Figure S24: Electrospray Ionization Mass Spectra of compound **2** (solid line) isolated from the 2:1 THF/CH_3CN labeling experiment and natural abundance compound **2** (dashed line). The result of majority triple ^{18}O incorporation conditions: **3** (1 equiv.), $NEt_4{}^{18}OH$ (2 equiv.), $H_2{}^{18}O$ (ca. 60 equiv.), $FcPF_6$ (4 equiv.), 2:1 THF/CH_3CN, r.t., 35 minutes.

9 Quantification of Isotopologue Ratio.

For a similar ESI-MS analysis, see [24]. The peak assignments for natural abundance **2** (1257.1 $m/z = LMn_4O_4(OAc)_2^+$ and **3** (1241.1 $m/z = LMn_4O_3(OAc)_2^+$)) were based on m/z values and theoretical isotope distribution. The theoretical isotope distribution was obtained by inputting the molecular formulas into the isotope distribution calculator program at http://www.sisweb.com/mstools/isotope.htm. For natural abundance **2**, the distributation is: 1257.1-100% relative abundance, 1258.1-69%, 1259.1-26%, 1260.1-7%, and 1261.1-1%. The same distribution is found for **3**. Therefore, for ^{18}O enriched samples, overlap of the expected isotope distributions for each ^{18}O isotopologue (separated by two m/z units) is expected. Moreover, both the parent (1257.1 m/z) and protonated (1258.1 m/z) species for **2** are observed in the ESI-MS spectrum with variable amounts of protonation from sample to sample (Figure S23). If crude **2** was taken from the water incorporation reaction, more protonation was observed; after fractionation with Et_2O and C_6H_6 less protonated **2** was observed. However, a small amount of adventitious protons in the ESI-MS line gave a variable amount of protonated complex and therefore both **2** and $\mathbf{2}_{\mathbf{H}^+}$ had to be taken into account in the isotopologue ratio calculations. From this, ten masses are expected: **2** at 1257.1, $\mathbf{2}_{\mathbf{H}^+}$ at 1258.1, **2*** at 1259.1, $\mathbf{2^*}_{\mathbf{H}^+}$ at 1260.1 through to $\mathbf{2^{****}}_{\mathbf{H}^+}$ at 1266.1 m/z.

To quantify the amount of each isotopologue of **2** and $\mathbf{2}_{\mathbf{H}^+}$, let pi represent the theoretical isotope distribution, with $p_1 = 0.69$, $p_2 = 0.26$, ... $p4 = 0.01$. Let T_{m+n} represent the observed relative abundance (Total peak height observed in the spectrum) at mass $m + n$, with m representing the first mass (1257.1) and n = 0,1,2,...9. Thus each value of $m + n$ represents one of the ten masses from **2** to $\mathbf{2^{****}}_{\mathbf{H}^+}$. Therefore, the relative abundance, or intensity, of each isotopologue of **2** and $\mathbf{2^*}_{\mathbf{H}^+}$, denoted I_{m+n}, is given by the equation:

$$I_{m+n} = T_{m+n} - \sum_{i=1}^{n} p_i \cdot I_{m+n-i}$$

From this equation, the intensity of each of the ten species can be calculated. For example, the intensity of **2***

(I_{m+2}) is the total, observed relative abundance at 1259.1 m/z (T_{m+2}) minus the 69% peak for $\mathbf{2^*_{H+}}$ ($p_1 \cdot I_{m+1}$), and the 26% peak for **2** ($p_2 \cdot I_m$):

$$I_{m+2} = T_{m+2} - (p_1 \cdot I_{m+1} + p_2 \cdot I_m)$$

These ten intensities were converted to mole fraction by dividing each intensity by the overall sum:

$$\chi_{m+n} = (I_{m+n})/(\sum_{n=0}^{9} I_{m+n})$$

The mole fraction of each isotopologue (**2**, **2***,...,**2******) is the sum of the mole fraction of each of the unprotonated isotopologues and their corresponding protonated isotopologue, with y = 0,1,2,3, and 4, representing the number of ^{18}O:

$$\chi_y = \chi_{m+n} + \chi_{m+n+1}$$

So the five mole fractions of **2** through **2******** are:

$$\chi_0 = \chi_m + \chi_{m+1},\ \chi_1 = \chi_{m+2} + \chi_{m+3},\ \chi_2 = \chi_{m+4} + \chi_{m+5},\ \chi_3 = \chi_{m+6} + \chi_{m+7},\ \chi_4 = \chi_{m+8} + \chi_{m+9}$$

The same is applicable to **3**, with n = 0,1,2,... 7 for **3** at 1241.1 m/z through $\mathbf{3^{***}_{H+}}$ at 1248.1 m/z.

Table S8: Isotopologue mole fractions for **2** and **3** isolated from the water incorporation and removal reactions, respectively.

χ_y	**2*[a]**	**3*[b]**
χ_0	0.09	0.28
χ_1	0.61	0.52
χ_2	0.17	0.15
χ_3	0.09	0.05
χ_4	0.04	–

[a] Conditions: **3**, $NMe_4{}^{18}OH$ (2 equiv.), $H_2{}^{18}O$ (20 equiv.),$FcPF_6$ (4 equiv.), 10:1 THF/CH_3CN, RT 35 min.
[b] Condtions: **2***, PMe_3 (10 equiv.), C_6H_6, RT ≥6 hours.

10 Calculation of Theoretical Isotopologue Distribution of 3.

By applying the expected statistical outcome of a specific water incorporation/O-atom transfer pathway to the experimental isotopologue distribution of **2** from the ESI-MS analysis above, one can determine if a certain mechanism of incorporation/removal is consistent with the experimentally observed isotopologue ratio of **3** (Scheme S1). Starting at the left side of Scheme S1, there are three possible mechanisms of incorporation: top selective, bottom selective, or not selective. Each gives its own isotopomer mixture of each isotopologue (isotopomer is used to denote the location of ^{18}O within the cubane, whereas isotopologue is used to denote the number of ^{18}O's).

For example, the singly labeled **2*** (61% of the distribution), will be 75% $\mathbf{2^{T}*}$ and 25% $\mathbf{2^{B}*}$ for a random water incorporation mechanism - three top positions to one bottom position. Applying this statistical outcome to

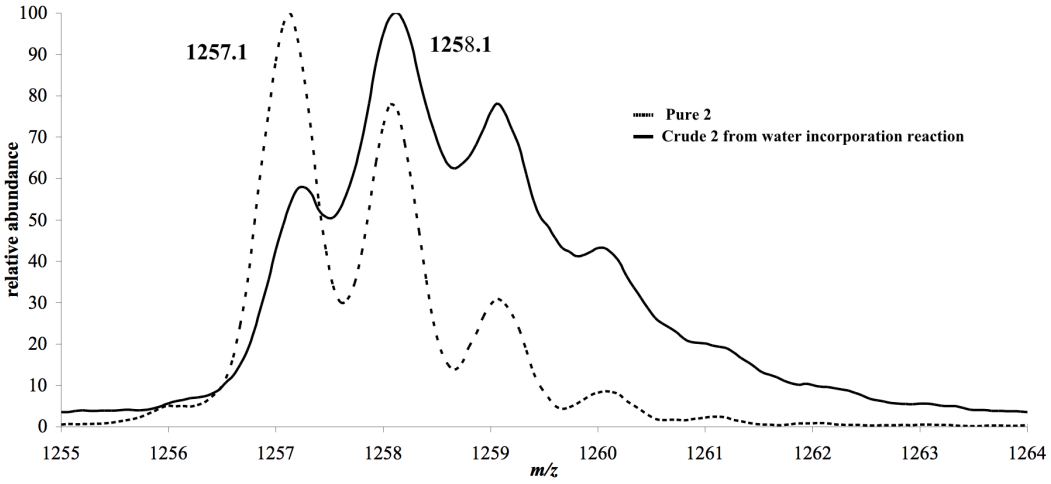

Figure S25: Electrospray Ionization Mass Spectra of pure compound **2** (dashed lines) and crude compound **2** isolated from the natural abundance H_2O control experiment (solid line). The 1257.1 and 1258.1 peaks correspond to the unprotonated and protonated mass with one acetate lost from the parent ion - $LMn_4O_4(OAc)_2^+$ and $[LMn_4O4(OAc)_2]H^+$. Natural abundance control experiment conditions: **3** (1 equiv.), NMe_4OH (2 equiv.), H_2O (ca. 30 equiv.), $FcPF_6$ (4 equiv.), THF/CH_3CN, RT, 30 minutes.

the 61% of **2*** gives 15.25% $\mathbf{2}^{\mathrm{T}}$* and 45.75% $\mathbf{2}^{\mathrm{B}}$* for the whole distribution of species. Taking these hypothetical distributions of **2** on to the O-atom transfer reaction gives five possible pathways: top/top, top/bottom, bottom/bottom, bottom/top, and random. The first term refers to water incorporation and the second term refers to O-atom transfer."Bottom" refers to the central, basal oxido position closest to the ligand framework. "Top" refers to the three other oxido sites on the cubane (those further from the ligand framework and therefore on the 'top'). "Random" represents random incorporation, random removal, or both; the calculated mole fractions are the same for all three cases. Applying each statistical outcome to all eight possible species of **2** gives the distribution of the four possible isotopologues of **3**. Summing up the percentages of each isotopologue gives the theoretical distribution of **3** that can be directly compared to the distribution of **3** experimentally determined from ESI-MS (Table S9).

Table S9: Experimental and calculated isotopologue percentages for various possible water incorporation/O-atom transfer mechanisms.

χ_y	Experimental	Bottom/Bottom	Top/Bottom	Bottom/Top	Top/Top	Random
χ_0	28%	70%	9%	9%	29.33%	24.25%
χ_1	52%	17%	61%	66.67%	52%	54.25%
χ_2	15%	9%	17%	17.33%	14.67%	15.25%
χ_3	5%	4%	13%	7%	4%	6.25%
Consistent	–	No	No	No	Yes	Yes

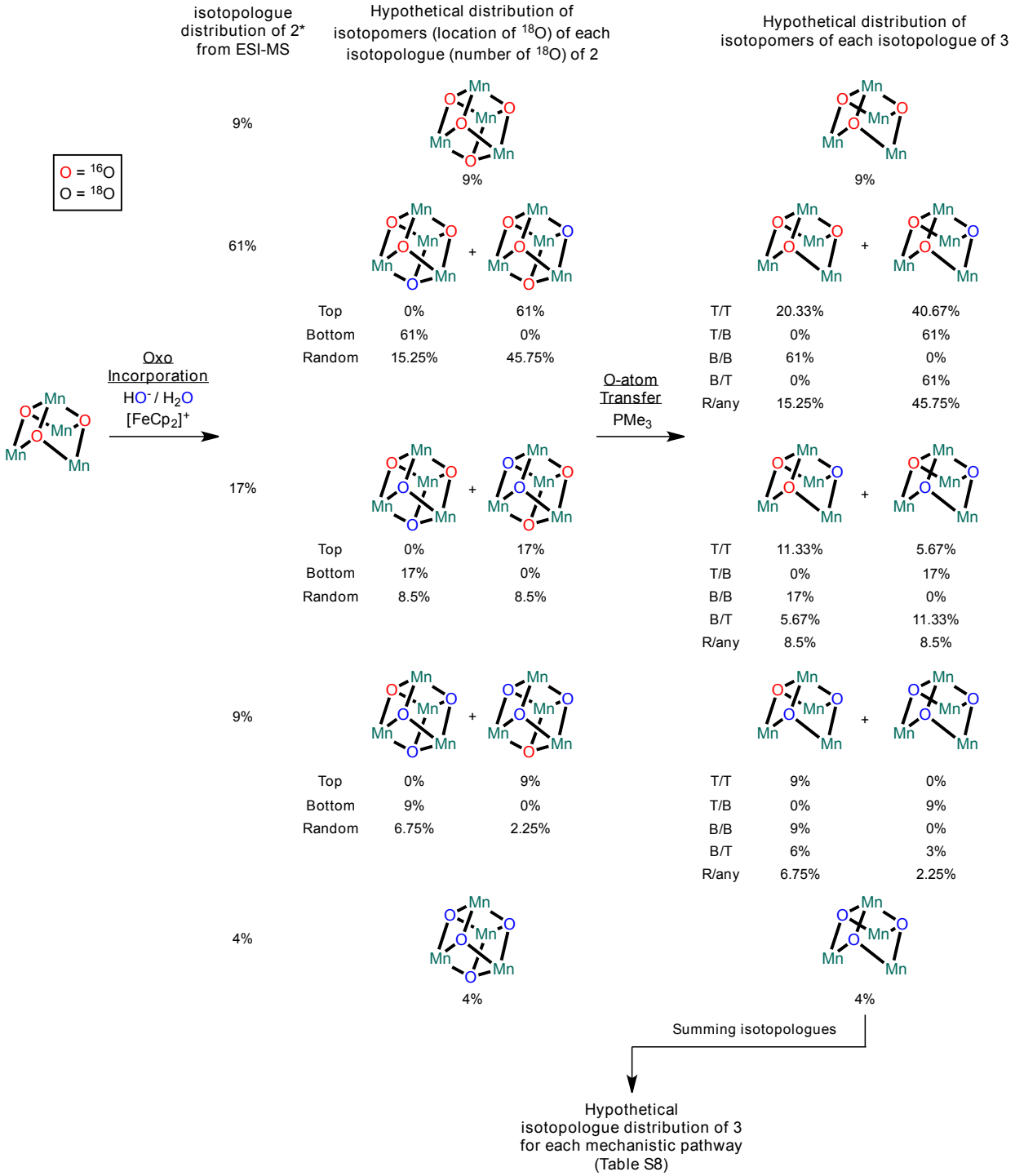

Scheme 1: Calculation of theoretical isotopologue distribution of **3** for each possible pathway of water incorporation and O-atom transfer. T=Top, B=Bottom, R=Random.

11 d_3-acetate Labeling Studies

11.1 4 + nBu$_4$NOAc-d_3.

In a glovebox, **4** (1.0 mg, 7.0x10^{-4} mmol) was dissolved in 10:1 THF/CH_3CN (1.0 mL) in a septum-capped 10 mL round-bottom flask. Separately, a 0.35 mM solution of nBu$_4$NOAc-d_3 in 10:1 THF/CH_3CN was prepared and 6 mL was taken up in a syringe. The solution of **4** in the flask and the syringe of acetate solution were taken to the ESI-MS room. The 6 mL of acetate solution was injected into the solution of **4** to give a 100 μM solution of **4** with 3 equivalents of d_3-acetate. Samples were taken directly from this flask and injected into the spectrometer.

11.2 2 + nBu$_4$NOAc-d_3.

In a glovebox, 2 (0.5 mg, 3.8x10^{-4} mmol) was dissolved in 10:1 THF/CH_3CN (1.9 mL) in a septum-capped 10 mL round-bottom flask. Separately, a 0.60 mM solution of nBu$_4$NOAc-d_3 in 10:1 THF/CH_3CN was prepared and 1.9 mL was taken up in a syringe. The solution of **2** in the flask and the syringe of acetate solution were taken to the ESI-MS room. The acetate solution was injected into the solution of **2** to give a 100 μM solution of **2** with 3 equivalents of d_3-acetate. Samples were taken directly from this flask and injected into the spectrometer.

11.3 5 + nBu$_4$NOAc-d_3.

In a glovebox, **5** (1.2 mg, 8.2x10^{-4} mmol) was dissolved in 10:1 THF/CH_3CN (1.2 mL) in a septum-capped 10 mL round-bottom flask. Separately, a 0.35 mM solution of nBu$_4$NOAc-d_3 in 10:1 THF/CH_3CN was prepared and 6 mL was taken up in a syringe. The solution of **5** in the flask and the syringe of acetate solution were taken to the ESI-MS room. The acetate solution was injected into the solution of **5** to give a 100 μM solution of **5** with 3 equivalents of d_3-acetate. Samples were taken directly from this flask and injected into the spectrometer.

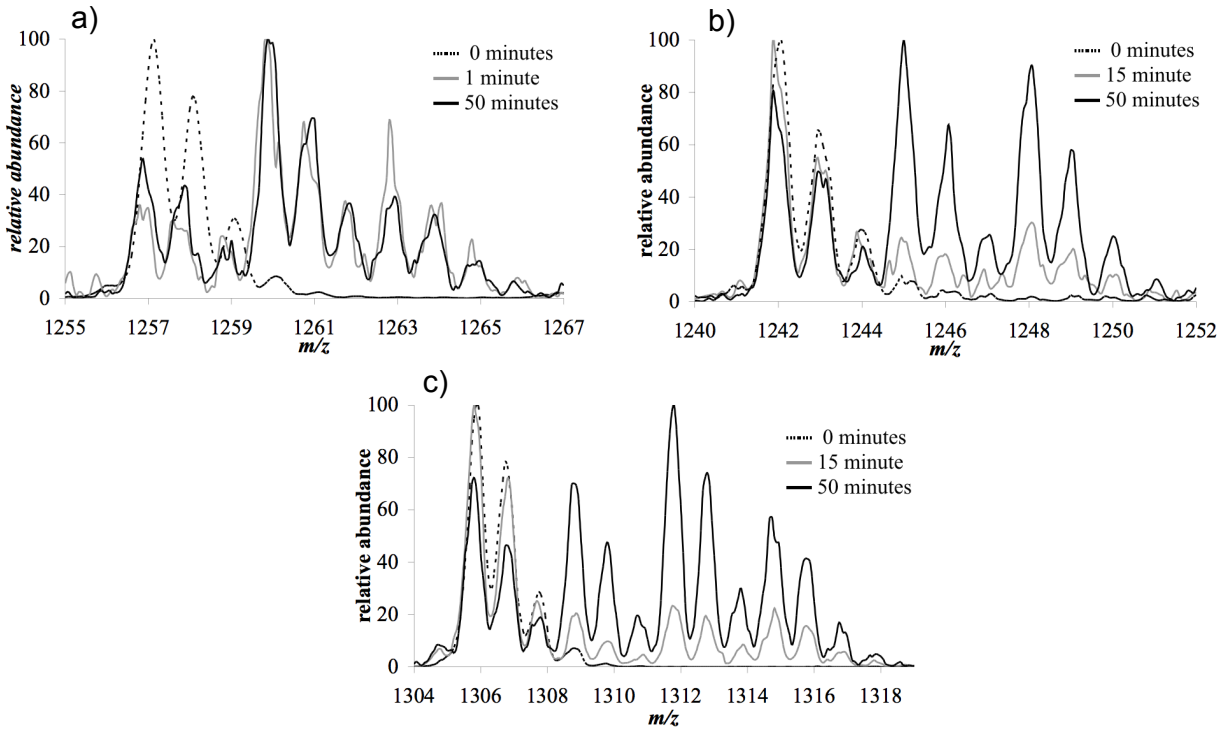

Figure S26: Electrospray Ionization Mass Spectra of 100 μM **2** (a), **4** (b) and **5** (c) after mixture with nBu$_4$NOAc-$_{d3}$ at 15 minute (grey line; 1 minute for **2**) and 50 minutes (black line). The unscrambled starting complexes are shown as '0 minute' spectra (dotted lines). Conditions: **2**, **4** or **5** (100 μM in 10:1 THF/CH_3CN), nBu$_4$NOAc-d_3 (3 equiv.), RT

12 Crystallographic Information

Table S10: Crystal and refinement data for complexes **3** and **5**.

	3	**5**
Empirical formula[a]	$C_{63}H_{48}N_6O_{12.09}Mn_4{\cdot}4(C_4H_8O)$	$C_{70}H_{61}F_3Mn_3N_7O_{17}SSc$
Formula wt	1590.45	1571.10
T (K)	100	100
a, Å	13.7255(6)	13.7160(7)
b, Å	18.1596(7)	15.8986(7)
c, Å	28.1662(11)	16.3736(8)
α, deg	90	73.250(2)
β, deg	92.620(2)	84.410(3)
γ, deg	90	72.393(2)
V, Å^3	7013.1(5)	3258.6(3)
Z	4	2
Cryst syst	Monoclinic	Triclinic
Space group	$P2_1/c$	$P\bar{1}$
d_{calcd}, g/cm^3	1.506	1.601
θ range, deg	1.83 to 26.43	1.77 to 43.86
μ, mm^{-1}	0.780	0.788
Abs cor	None	Semi-empirical from equivalents
GOF	1.277	1.270
$R1$;[a] $wR2$[b] ($I > 2\sigma(I)$)	0.0569, 0.0549	0.0464, 0.1091

[a] $R1 = \sum ||F_0| - |F_c|| / \sum |F_0|$
[b] $wR2 = \{\sum [w(F_0^2 - F_c^2)^2] / \sum [w(F_0^2)^2]\}^{1/2}$

12.1 Special Refinement Details: Compound 3

Crystals were mounted on a loop then placed on the diffractometer under a nitrogen stream at 100K. The asymmetric unit contains four molecules of THF and the largest peaks in the final difference Fourier map are in the area of these, suggesting disorder. This was not modeled. Additionally, the Fourier map contained a peak suggesting an oxygen capping the Mn_4O_3 partial cubane structure (Figure S27). This oxygen was assigned a fixed temperature factor ($U = 0.050$) and was included in the final least squares refinement with position and occupancy free to refine. The refined occupancy was equal to 0.09.

Refinement of $F2$ against ALL reflections. The weighted R-factor (wR) and goodness of fit (S) are based on $F2$, conventional R-factors (R) are based on F, with F set to zero for negative $F2$. The threshold expression of $F2 > 2\sigma(F2)$ is used only for calculating R-factors(gt) etc. and is not relevant to the choice of reflections for refinement. R-factors based on $F2$ are statistically about twice as large as those based on F, and R-factors based on ALL data will be even larger.

All esds (except the esd in the dihedral angle between two l.s. planes) are estimated using the full covariance matrix. The cell esds are taken into account individually in the estimation of esds in distances, angles and torsion angles; correlations between esds in cell parameters are only used when they are defined by crystal symmetry. An approximate (isotropic) treatment of cell esds is used for estimating esds involving l.s. planes.

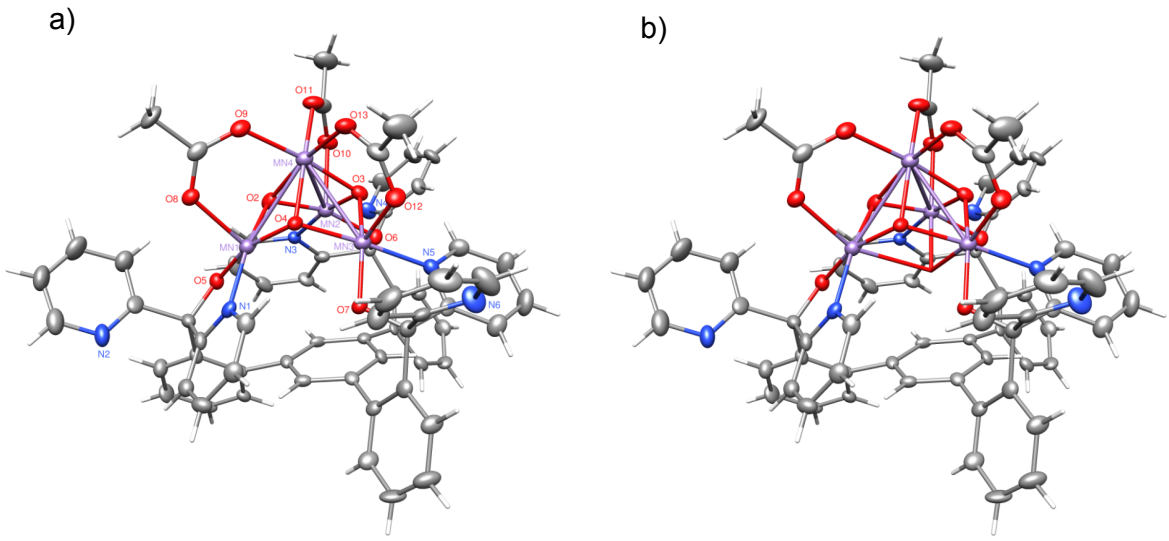

Figure S27: Structural drawings of **3** where the oxygen atom with a population of 0.09 is a) not included and b) included.

Table S11: Atomic coordinates (x 10^4) and equivalent isotropic displacement parameters (Å^2 x 10^3) for **3** (CCDC 840141). $U(eq)$ is defined as the trace of the orthogonalized U^{ij} tensor

	x	y	z	Ueq	Occ
Mn(1)	1839(1)	2212(1)	8820(1)	22(1)	1
Mn(2)	2926(1)	3652(1)	8459(1)	22(1)	1
Mn(3)	767(1)	3262(1)	8032(1)	21(1)	1
Mn(4)	2406(1)	2428(1)	7863(1)	22(1)	1
O(1A)	1440(20)	3452(16)	8656(10)	50	0.090(4)
O(2)	2937(2)	2649(1)	8582(1)	24(1)	1
O(3)	2075(2)	3464(1)	7908(1)	22(1)	1
O(4)	1213(2)	2314(1)	8208(1)	19(1)	1
O(5)	2242(2)	2358(1)	9453(1)	23(1)	1
O(6)	2641(2)	4659(1)	8478(1)	20(1)	1
O(7)	-408(2)	3192(1)	8329(1)	20(1)	1
O(8)	2356(2)	1136(1)	8653(1)	25(1)	1
O(9)	2765(2)	1374(1)	7901(1)	28(1)	1
O(10)	4174(2)	3587(1)	8048(1)	28(1)	1
O(11)	3665(2)	2638(1)	7584(1)	29(1)	1
O(12)	326(2)	2938(1)	7352(1)	28(1)	1
O(13)	1641(2)	2250(1)	7206(1)	28(1)	1

Continued on next page

Table S11 – *Continued from previous page*

	x	*y*	*z*	*Ueq*	*Occ*
N(1)	582(2)	1915(2)	9132(1)	21(1)	1
N(2)	1607(3)	864(2)	10226(1)	33(1)	1
N(3)	3594(2)	3880(2)	9098(1)	18(1)	1
N(4)	4842(3)	5600(2)	8832(1)	29(1)	1
N(5)	257(2)	4292(2)	7892(1)	21(1)	1
N(6)	-2025(2)	3566(2)	7367(1)	33(1)	1
C(1)	-285(3)	1798(2)	8908(1)	24(1)	1
C(2)	-1095(3)	1650(2)	9153(1)	26(1)	1
C(3)	-1019(3)	1611(2)	9644(1)	28(1)	1
C(4)	-133(3)	1728(2)	9875(1)	25(1)	1
C(5)	667(3)	1890(2)	9612(1)	21(1)	1
C(6)	1678(3)	2054(2)	9810(1)	23(1)	1
C(7)	2146(3)	1308(2)	9966(1)	27(1)	1
C(8)	3087(3)	1143(2)	9839(1)	39(1)	1
C(9)	3479(4)	466(2)	9993(2)	48(1)	1
C(10)	2929(4)	9(2)	10256(2)	46(1)	1
C(11)	2005(4)	227(2)	10365(1)	43(1)	1
C(12)	1701(3)	2600(2)	10227(1)	21(1)	1
C(13)	2103(3)	2399(2)	10672(1)	28(1)	1
C(14)	2224(3)	2881(2)	11048(1)	31(1)	1
C(15)	1947(3)	3599(2)	10979(1)	25(1)	1
C(16)	1552(3)	3823(2)	10540(1)	21(1)	1
C(17)	1407(3)	3339(2)	10164(1)	18(1)	1
C(18)	3904(3)	3381(2)	9424(1)	27(1)	1
C(19)	4195(3)	3576(2)	9877(1)	31(1)	1
C(20)	4170(3)	4311(2)	9996(1)	29(1)	1
C(21)	3883(3)	4831(2)	9663(1)	25(1)	1
C(22)	3571(3)	4601(2)	9213(1)	22(1)	1
C(23)	3174(3)	5096(2)	8809(1)	18(1)	1
C(24)	4054(3)	5445(2)	8565(1)	18(1)	1
C(25)	3975(3)	5602(2)	8088(1)	27(1)	1
C(26)	4744(3)	5929(2)	7877(1)	32(1)	1
C(27)	5558(3)	6091(2)	8145(2)	35(1)	1
C(28)	5582(3)	5919(2)	8619(2)	36(1)	1

Continued on next page

Table S11 – *Continued from previous page*

	x	*y*	*z*	*Ueq*	*Occ*
C(29)	2506(3)	5686(2)	9009(1)	16(1)	1
C(30)	2834(3)	6409(2)	9044(1)	24(1)	1
C(31)	2260(3)	6979(2)	9194(1)	28(1)	1
C(32)	1331(3)	6833(2)	9313(1)	25(1)	1
C(33)	992(3)	6117(2)	9292(1)	22(1)	1
C(34)	1568(3)	5530(2)	9152(1)	16(1)	1
C(35)	765(3)	4863(2)	7733(1)	27(1)	1
C(36)	318(3)	5512(2)	7600(1)	33(1)	1
C(37)	-673(3)	5566(2)	7640(1)	39(1)	1
C(38)	-1195(3)	4985(2)	7816(1)	30(1)	1
C(39)	-702(3)	4347(2)	7945(1)	22(1)	1
C(40)	-1156(3)	3655(2)	8153(1)	20(1)	1
C(41)	-1743(3)	3225(2)	7766(1)	21(1)	1
C(42)	-1926(3)	2489(2)	7851(1)	32(1)	1
C(43)	-2406(3)	2085(2)	7503(2)	37(1)	1
C(44)	-2670(3)	2422(2)	7082(2)	38(1)	1
C(45)	-2470(3)	3146(2)	7030(1)	42(1)	1
C(46)	-1820(3)	3870(2)	8562(1)	21(1)	1
C(47)	-2809(3)	3937(2)	8474(1)	26(1)	1
C(48)	-3447(3)	4064(2)	8830(2)	34(1)	1
C(49)	-3072(3)	4121(2)	9290(2)	31(1)	1
C(50)	-2088(3)	4080(2)	9384(1)	26(1)	1
C(51)	-1428(3)	3977(2)	9032(1)	19(1)	1
C(52)	-376(3)	4037(2)	9174(1)	17(1)	1
C(53)	41(3)	3579(2)	9524(1)	19(1)	1
C(54)	979(3)	3708(2)	9717(1)	18(1)	1
C(55)	1488(3)	4318(2)	9562(1)	17(1)	1
C(56)	1101(3)	4794(2)	9213(1)	17(1)	1
C(57)	162(3)	4640(2)	9029(1)	19(1)	1
C(58)	2712(3)	960(2)	8268(2)	27(1)	1
C(59)	3136(3)	196(2)	8220(1)	40(1)	1
C(60)	4271(3)	3139(2)	7717(1)	29(1)	1
C(61)	5207(3)	3167(2)	7450(1)	45(1)	1
C(62)	785(3)	2475(2)	7117(1)	27(1)	1

Continued on next page

Table S11 – *Continued from previous page*

	x	*y*	*z*	*Ueq*	*Occ*
C(63)	218(3)	2164(2)	6687(1)	50(1)	1
O(70B)	2852(3)	-238(2)	2014(1)	73(1)	1
C(71B)	2098(4)	-93(3)	1669(2)	69(2)	1
C(72B)	2048(5)	750(3)	1629(2)	93(2)	1
C(73B)	3099(4)	978(3)	1687(2)	85(2)	1
C(74B)	3481(4)	414(3)	2033(2)	90(2)	1
O(70C)	5332(4)	2255(3)	550(3)	196(3)	1
C(71C)	4920(5)	2007(4)	981(2)	118(3)	1
C(72C)	5308(6)	1324(5)	1101(2)	171(4)	1
C(73C)	5948(7)	1111(4)	759(3)	170(5)	1
C(74C)	5851(6)	1618(6)	377(3)	149(3)	1
O(70D)	8686(3)	1000(2)	789(1)	91(1)	1
C(71D)	9221(5)	1277(3)	1166(2)	108(3)	1
C(72D)	9388(4)	691(3)	1494(2)	70(2)	1
C(73D)	9573(4)	83(2)	1181(2)	62(2)	1
C(74D)	8988(4)	252(3)	743(2)	81(2)	1
O(70E)	3788(5)	8561(2)	821(2)	206(3)	1
C(71E)	3822(4)	7837(3)	881(2)	74(2)	1
C(72E)	4279(4)	7754(3)	1362(2)	87(2)	1
C(73E)	4869(4)	8416(3)	1423(2)	84(2)	1
C(74E)	4564(6)	8919(3)	1096(3)	195(5)	1

Table S12: Anisotropic displacement parameters (Å^2 x 10^4) for **3** (CCDC 840141). The anisotropic displacement factor exponent takes the form: -$2\pi^2[h^2a*^2U^{11} + \ldots + 2hka*b*U^{12}]$

	U^{11}	U^{22}	U^{33}	U^{23}	U^{13}	U^{12}
Mn(1)	245(4)	181(4)	236(4)	-6(3)	42(3)	12(3)
Mn(2)	243(4)	192(4)	232(4)	-26(3)	42(3)	-1(3)

Continued on next page

Table S12 – *Continued from previous page*

	U^{11}	U^{22}	U^{33}	U^{23}	U^{13}	U^{12}
Mn(3)	222(4)	203(4)	213(4)	-30(3)	33(3)	6(3)
Mn(4)	247(4)	198(4)	230(4)	-37(3)	40(3)	5(3)
O(2)	261(18)	119(15)	342(18)	0(13)	51(14)	13(13)
O(3)	252(18)	236(17)	172(16)	-8(13)	23(13)	-19(13)
O(4)	223(17)	171(15)	170(16)	-23(12)	20(13)	33(13)
O(5)	283(18)	174(16)	236(17)	18(13)	23(14)	1(14)
O(6)	237(18)	165(15)	186(16)	-21(13)	-48(13)	11(13)
O(7)	218(18)	177(16)	213(16)	-7(13)	28(14)	36(13)
O(8)	283(19)	173(16)	297(19)	-36(14)	51(15)	9(14)
O(9)	310(20)	244(17)	266(18)	-86(15)	9(15)	30(15)
O(10)	286(19)	313(18)	257(18)	-56(15)	67(15)	-71(15)
O(11)	280(20)	337(19)	247(18)	-85(15)	85(15)	5(15)
O(12)	360(20)	244(18)	233(18)	-75(14)	-15(15)	26(15)
O(13)	280(20)	322(18)	254(18)	-44(14)	67(15)	37(16)
N(1)	210(20)	116(19)	300(20)	-6(17)	29(18)	23(16)
N(2)	490(30)	180(20)	310(20)	37(19)	-10(20)	0(20)
N(3)	200(20)	190(20)	160(20)	6(16)	22(16)	18(16)
N(4)	250(20)	350(20)	290(20)	20(18)	0(20)	-79(19)
N(5)	240(20)	200(20)	190(20)	7(16)	10(18)	-12(18)
N(6)	410(30)	350(20)	240(20)	-50(20)	-106(19)	-90(20)
C(1)	270(30)	170(20)	280(30)	-30(20)	-40(20)	-40(20)
C(2)	250(30)	180(20)	350(30)	-10(20)	20(20)	-50(20)
C(3)	310(30)	210(30)	320(30)	-20(20)	150(20)	-30(20)
C(4)	320(30)	160(20)	270(30)	10(20)	60(20)	20(20)
C(5)	300(30)	130(20)	200(30)	20(20)	-10(20)	10(20)
C(6)	310(30)	170(20)	200(30)	20(20)	90(20)	30(20)
C(7)	380(30)	270(30)	150(30)	-30(20)	-30(20)	50(20)
C(8)	400(40)	330(30)	430(30)	40(20)	20(30)	70(30)
C(9)	430(40)	390(30)	630(40)	10(30)	-10(30)	160(30)
C(10)	640(40)	270(30)	470(40)	80(30)	-10(30)	100(30)
C(11)	680(40)	260(30)	340(30)	30(20)	-50(30)	10(30)
C(12)	260(30)	200(30)	170(30)	40(20)	10(20)	-10(20)
C(13)	350(30)	210(30)	280(30)	10(20)	-20(20)	20(20)
C(14)	370(30)	350(30)	190(30)	50(20)	-70(20)	30(20)

Continued on next page

Table S12 – *Continued from previous page*

	U^{11}	U^{22}	U^{33}	U^{23}	U^{13}	U^{12}
C(15)	250(30)	300(30)	210(30)	-70(20)	80(20)	-70(20)
C(16)	220(30)	240(30)	170(30)	30(20)	50(20)	10(20)
C(17)	210(30)	160(20)	170(30)	-10(20)	40(20)	-10(20)
C(18)	250(30)	200(30)	370(30)	80(20)	-10(20)	40(20)
C(19)	310(30)	330(30)	280(30)	70(20)	-90(20)	-70(20)
C(20)	250(30)	420(30)	190(30)	40(20)	0(20)	-90(20)
C(21)	330(30)	270(30)	140(30)	-50(20)	10(20)	-30(20)
C(22)	250(30)	200(30)	230(30)	-40(20)	90(20)	0(20)
C(23)	230(30)	140(20)	160(30)	-10(20)	0(20)	20(20)
C(24)	210(30)	160(20)	190(30)	-40(20)	50(20)	40(20)
C(25)	360(30)	260(30)	190(30)	0(20)	-30(20)	20(20)
C(26)	420(40)	360(30)	180(30)	60(20)	110(30)	0(30)
C(27)	320(30)	380(30)	350(30)	100(20)	150(30)	-70(20)
C(28)	210(30)	430(30)	440(30)	60(30)	10(30)	-100(20)
C(29)	220(30)	150(20)	130(20)	-2(19)	0(20)	10(20)
C(30)	270(30)	230(30)	230(30)	-10(20)	50(20)	10(20)
C(31)	390(30)	160(20)	300(30)	-20(20)	50(20)	-40(20)
C(32)	340(30)	220(30)	210(30)	-50(20)	70(20)	90(20)
C(33)	230(30)	280(30)	160(30)	40(20)	10(20)	-20(20)
C(34)	230(30)	180(20)	80(20)	29(19)	-20(20)	40(20)
C(35)	260(30)	260(30)	300(30)	-40(20)	30(20)	-50(20)
C(36)	270(30)	260(30)	450(30)	60(20)	-70(20)	-30(20)
C(37)	460(40)	240(30)	450(30)	60(20)	-120(30)	50(30)
C(38)	260(30)	240(30)	370(30)	-40(20)	-60(20)	-10(20)
C(39)	250(30)	230(30)	160(30)	-60(20)	-90(20)	50(20)
C(40)	170(30)	220(20)	220(30)	0(20)	-20(20)	0(20)
C(41)	180(30)	240(30)	230(30)	-40(20)	50(20)	60(20)
C(42)	350(30)	240(30)	380(30)	-60(20)	-80(20)	0(20)
C(43)	330(30)	220(30)	550(40)	-70(30)	70(30)	30(20)
C(44)	410(30)	400(30)	350(30)	-200(30)	60(30)	-130(30)
C(45)	440(30)	520(30)	300(30)	70(30)	-10(30)	-180(30)
C(46)	250(30)	120(20)	270(30)	0(20)	20(20)	-10(20)
C(47)	190(30)	300(30)	280(30)	-90(20)	-20(20)	0(20)
C(48)	200(30)	410(30)	430(30)	-140(30)	60(30)	10(20)

Continued on next page

Table S12 – *Continued from previous page*

	U^{11}	U^{22}	U^{33}	U^{23}	U^{13}	U^{12}
C(49)	240(30)	390(30)	320(30)	-160(20)	130(20)	-10(20)
C(50)	270(30)	260(30)	260(30)	-80(20)	-20(20)	0(20)
C(51)	200(30)	120(20)	250(30)	-20(19)	30(20)	8(19)
C(52)	240(30)	130(20)	140(30)	-38(19)	30(20)	0(20)
C(53)	170(30)	180(20)	210(30)	-50(20)	60(20)	-20(20)
C(54)	280(30)	120(20)	140(20)	-22(19)	40(20)	30(20)
C(55)	110(20)	250(30)	160(20)	-50(20)	11(19)	10(20)
C(56)	200(30)	180(20)	150(30)	-20(20)	40(20)	30(20)
C(57)	250(30)	200(20)	120(20)	42(19)	20(20)	30(20)
C(58)	250(30)	220(30)	340(30)	-90(20)	-30(20)	20(20)
C(59)	490(40)	190(30)	510(30)	-80(20)	30(30)	130(20)
C(60)	220(30)	390(30)	260(30)	30(20)	60(20)	80(20)
C(61)	330(30)	640(30)	410(30)	-10(30)	100(30)	30(30)
C(62)	370(30)	260(30)	190(30)	-60(20)	40(20)	-60(20)
C(63)	350(30)	710(40)	440(30)	-170(30)	-10(30)	0(30)
O(70B)	840(30)	670(30)	650(30)	50(20)	-150(20)	-70(20)
C(71B)	850(50)	700(40)	500(40)	20(30)	-250(30)	-190(40)
C(72B)	1320(70)	430(40)	1050(50)	110(40)	70(50)	110(40)
C(73B)	760(50)	630(40)	1100(50)	250(40)	-500(40)	-90(40)
C(74B)	1070(60)	420(40)	1170(50)	130(40)	-360(40)	-310(40)
O(70C)	1400(60)	1590(60)	2920(90)	1230(60)	510(50)	630(50)
C(71C)	1630(80)	720(50)	1250(70)	330(50)	590(60)	160(60)
C(72C)	2470(110)	1710(90)	990(60)	170(60)	600(60)	1520(80)
C(73C)	3000(140)	1350(80)	710(60)	80(50)	-130(70)	1230(80)
C(74C)	720(70)	2300(120)	1440(80)	-340(90)	-80(60)	-400(70)
O(70D)	930(40)	890(40)	870(30)	40(30)	-280(30)	190(30)
C(71D)	2170(90)	520(50)	560(50)	-110(40)	140(50)	250(50)
C(72D)	960(50)	550(40)	610(40)	-50(40)	60(40)	190(40)
C(73D)	780(50)	420(40)	660(40)	-20(30)	110(40)	120(30)
C(74D)	1480(70)	550(40)	380(40)	-60(30)	-140(40)	-230(40)

Continued on next page

Table S12 – *Continued from previous page*

	U^{11}	U^{22}	U^{33}	U^{23}	U^{13}	U^{12}
O(70E)	3970(100)	360(30)	1660(50)	50(30)	-1820(50)	250(40)
C(71E)	560(40)	790(50)	840(50)	-210(40)	-280(30)	210(40)
C(72E)	890(50)	1120(60)	580(40)	-50(40)	-80(40)	-70(50)
C(73E)	1050(60)	500(40)	930(50)	-10(40)	-480(40)	-270(40)
C(74E)	2860(120)	610(60)	2190(100)	210(60)	-1900(90)	-230(60)

12.2 Special Refinement Details: Compound 5

Crystals were grown by vapor diffusion of diethyl ether into an acetonitrile solution of **5** at room temperature, then mounted on a fiber using Paratone oil and then placed on the diffractometer under a nitrogen stream at 100 K.

The triflate anion bound to scandium is disordered, and populations were employed to model the ion in two positions. Restraints were used to treat the distances, angles, and displacement parameters of the ion. A molecule of acetonitrile and a molecule of diethyl ether were located in the structure.

Refinement of $F2$ against ALL reflections. The weighted R-factor (wR) and goodness of fit (S) are based on $F2$, conventional R-factors (R) are based on F, with F set to zero for negative $F2$. The threshold expression of $F2 > 2\sigma(F2)$ is used only for calculating R-factors(gt) etc. and is not relevant to the choice of reflections for refinement. R-factors based on $F2$ are statistically about twice as large as those based on F, and R-factors based on ALL data will be even larger.

All esds (except the esd in the dihedral angle between two l.s. planes) are estimated using the full covariance matrix. The cell esds are taken into account individually in the estimation of esds in distances, angles and torsion angles; correlations between esds in cell parameters are only used when they are defined by crystal symmetry. An approximate (isotropic) treatment of cell esds is used for estimating esds involving l.s. planes.

Table S13: Atomic coordinates (x 10^4) and equivalent isotropic displacement parameters (Å^2 x 10^3) for **5** (CCDC 901808). $U(eq)$ is defined as the trace of the orthogonalized U^{ij} tensor

	x	y	z	Ueq
Mn(1)	3027(1)	2303(1)	7077(1)	7(1)
Mn(2)	2144(1)	1276(1)	8501(1)	7(1)
Mn(3)	894(1)	2858(1)	7355(1)	7(1)
Sc(4)	2249(1)	3162(1)	8559(1)	8(1)

Continued on next page

Table S13 – *Continued from previous page*

	x	y	z	Ueq
O(1)	2023(1)	3336(1)	7208(1)	8(1)
O(3)	1163(1)	2411(1)	8509(1)	8(1)
O(4)	1932(1)	1758(1)	7301(1)	8(1)
O(2)	3142(1)	1884(1)	8277(1)	8(1)
O(5)	2413(1)	4020(1)	9346(1)	14(1)
O(13)	-40(1)	4016(1)	7458(1)	11(1)
O(11)	2342(1)	922(1)	9728(1)	11(1)
O(9)	4115(1)	2878(1)	6966(1)	11(1)
O(8)	3586(1)	3530(1)	8039(1)	13(1)
O(10)	2359(1)	2293(1)	9824(1)	14(1)
O(12)	900(1)	4298(1)	8338(1)	13(1)
C(4)	4185(1)	3372(1)	7439(1)	11(1)
C(6)	2439(1)	1459(1)	10142(1)	11(1)
C(2)	125(1)	4510(1)	7890(1)	11(1)
C(1)	-684(1)	5400(1)	7855(1)	18(1)
C(5)	2671(1)	1044(1)	11072(1)	20(1)
C(3)	5070(1)	3769(1)	7255(1)	17(1)
O(15)	3022(1)	185(1)	8383(1)	9(1)
O(14)	2869(1)	2588(1)	5916(1)	9(1)
O(16)	-116(1)	2312(1)	7394(1)	9(1)
N(1)	4157(1)	1221(1)	6821(1)	9(1)
N(3)	445(1)	3366(1)	6097(1)	9(1)
N(2)	1166(1)	473(1)	8804(1)	9(1)
C(13)	988(1)	1352(1)	5825(1)	10(1)
C(8)	2040(1)	1098(1)	5648(1)	9(1)
C(12)	562(1)	853(1)	6538(1)	10(1)
C(14)	2406(1)	1600(1)	4810(1)	10(1)
C(11)	1207(1)	69(1)	7071(1)	10(1)
C(15)	3174(1)	2054(1)	4675(1)	9(1)
C(21)	3202(1)	-1325(1)	8293(1)	10(1)
C(27)	-1259(1)	1938(1)	6653(1)	10(1)
C(26)	-577(1)	1069(1)	6649(1)	10(1)
C(9)	2664(1)	316(1)	6198(1)	10(1)
C(10)	2260(1)	-198(1)	6917(1)	10(1)

Continued on next page

Table S13 – *Continued from previous page*

	x	y	z	Ueq
C(20)	2958(1)	-1089(1)	7422(1)	10(1)
C(16)	3429(1)	2459(1)	3836(1)	13(1)
C(25)	3414(1)	-1733(1)	6963(1)	14(1)
C(31)	-998(1)	356(1)	6695(1)	14(1)
C(19)	1902(1)	1620(1)	4096(1)	13(1)
C(30)	-2050(1)	495(1)	6678(1)	16(1)
C(22)	3853(1)	-2196(1)	8670(1)	15(1)
C(24)	4065(1)	-2595(1)	7346(1)	17(1)
C(17)	2917(1)	2471(1)	3134(1)	15(1)
C(28)	-2310(1)	2076(1)	6603(1)	13(1)
C(18)	2137(1)	2060(1)	3267(1)	15(1)
C(23)	4282(1)	-2828(1)	8204(1)	18(1)
C(29)	-2707(1)	1366(1)	6600(1)	15(1)
C(33)	2805(1)	-640(1)	8834(1)	9(1)
C(32)	3670(1)	2188(1)	5419(1)	9(1)
C(34)	-888(1)	2717(1)	6774(1)	9(1)
C(45)	-438(1)	3223(1)	5964(1)	10(1)
C(35)	4332(1)	1305(1)	5981(1)	9(1)
C(40)	1655(1)	-430(1)	8965(1)	9(1)
C(37)	5641(1)	-124(1)	6274(1)	13(1)
C(39)	4723(1)	484(1)	7392(1)	10(1)
C(46)	-856(1)	3510(1)	5158(1)	14(1)
C(41)	1129(1)	-1084(1)	9190(1)	12(1)
C(38)	5457(1)	-208(1)	7139(1)	13(1)
C(48)	564(1)	4106(1)	4620(1)	16(1)
C(43)	-436(1)	138(1)	9048(1)	14(1)
C(49)	925(1)	3816(1)	5442(1)	12(1)
C(44)	139(1)	754(1)	8858(1)	11(1)
C(36)	5080(1)	652(1)	5686(1)	11(1)
C(42)	66(1)	-792(1)	9224(1)	15(1)
C(47)	-339(1)	3941(1)	4478(1)	17(1)
C(50)	4341(1)	2843(1)	5088(1)	10(1)
C(56)	3350(1)	-981(1)	9698(1)	10(1)
N(5)	2839(1)	-1287(1)	10401(1)	14(1)

Continued on next page

Table S13 – *Continued from previous page*

	x	y	z	Ueq
N(4)	5338(1)	2472(1)	4964(1)	15(1)
N(6)	-2136(1)	4254(1)	6635(1)	15(1)
C(62)	-1737(1)	3411(1)	7137(1)	11(1)
C(63)	-1991(1)	3146(1)	7998(1)	14(1)
C(60)	4817(1)	-1178(1)	10494(1)	18(1)
C(61)	4344(1)	-928(1)	9718(1)	16(1)
C(51)	3889(1)	3784(1)	4917(1)	15(1)
C(66)	-2774(1)	4870(1)	7006(1)	20(1)
C(64)	-2663(1)	3789(1)	8366(1)	19(1)
C(52)	4494(1)	4363(1)	4596(1)	19(1)
C(58)	3311(1)	-1519(1)	11152(1)	18(1)
C(59)	4281(1)	-1470(1)	11230(1)	16(1)
C(53)	5531(1)	3987(1)	4475(1)	20(1)
C(65)	-3051(1)	4677(1)	7858(1)	20(1)
C(54)	5919(1)	3041(1)	4668(1)	18(1)
O(17)	8233(1)	2776(1)	3602(1)	21(1)
C(71)	8830(1)	1256(1)	4497(1)	28(1)
C(70)	8943(1)	1899(1)	3645(1)	24(1)
C(69)	8254(1)	3394(1)	2775(1)	25(1)
C(68)	7496(1)	4298(1)	2760(1)	29(1)
N(7)	372(1)	2336(1)	1620(1)	42(1)
C(72)	-41(2)	3818(2)	382(1)	62(1)
C(74)	189(1)	2984(1)	1068(1)	36(1)
F(2)	3996(1)	5023(1)	10286(1)	48(1)
F(3)	4043(1)	4961(1)	8986(1)	40(1)
S(1A)	3064(1)	3911(1)	10048(1)	17(1)
O(6A)	2505(1)	3994(1)	10817(1)	38(1)
O(7A)	4002(1)	3188(1)	10117(1)	33(1)
C(7A)	3458(1)	4960(1)	9677(1)	27(1)
F(1A)	2652(1)	5702(1)	9492(1)	50(1)
S(1B)	2716(4)	4218(3)	10108(3)	19(1)
O(6B)	2845(17)	3467(11)	10851(8)	61(7)
O(7B)	2131(8)	5099(7)	10181(8)	33(1)
C(7B)	4006(9)	4326(10)	9803(11)	27(1)

Continued on next page

Table S13 – *Continued from previous page*

	x	y	z	Ueq
F(1B)	4626(9)	3529(12)	9707(9)	76(5)

Table S14: Anisotropic displacement parameters (Å^2 x 10^4) for **5** (CCDC 901808). The anisotropic displacement factor exponent takes the form: -$2\pi^2[h^2a*^2\,U^{11} + \ldots + 2hka*b*\,U^{12}]$

	U^{11}	U^{22}	U^{33}	U^{23}	U^{13}	U^{12}
Mn(1)	6(1)	8(1)	7(1)	-2(1)	1(1)	-2(1)
Mn(2)	6(1)	8(1)	7(1)	-2(1)	0(1)	-2(1)
Mn(3)	6(1)	8(1)	7(1)	-2(1)	0(1)	-2(1)
Sc(4)	8(1)	9(1)	8(1)	-3(1)	0(1)	-2(1)
O(1)	7(1)	8(1)	9(1)	-2(1)	0(1)	-2(1)
O(3)	8(1)	10(1)	8(1)	-2(1)	0(1)	-2(1)
O(4)	7(1)	9(1)	8(1)	-3(1)	0(1)	-2(1)
O(2)	7(1)	10(1)	8(1)	-2(1)	0(1)	-3(1)
O(5)	16(1)	16(1)	14(1)	-7(1)	-3(1)	-4(1)
O(13)	9(1)	11(1)	12(1)	-5(1)	-1(1)	-1(1)
O(11)	13(1)	12(1)	8(1)	-2(1)	-1(1)	-4(1)
O(9)	9(1)	13(1)	11(1)	-3(1)	1(1)	-4(1)
O(8)	12(1)	15(1)	14(1)	-6(1)	2(1)	-6(1)
O(10)	18(1)	14(1)	10(1)	-3(1)	-1(1)	-5(1)
O(12)	11(1)	13(1)	15(1)	-6(1)	-2(1)	-2(1)
C(4)	9(1)	11(1)	13(1)	-2(1)	-1(1)	-4(1)
C(6)	10(1)	14(1)	9(1)	-2(1)	0(1)	-3(1)
C(2)	9(1)	11(1)	12(1)	-4(1)	1(1)	-2(1)
C(1)	14(1)	15(1)	24(1)	-10(1)	-3(1)	2(1)
C(5)	27(1)	22(1)	9(1)	-2(1)	-5(1)	-5(1)
C(3)	13(1)	17(1)	24(1)	-5(1)	2(1)	-9(1)
O(15)	8(1)	8(1)	10(1)	-1(1)	1(1)	-3(1)
O(14)	7(1)	11(1)	8(1)	-3(1)	1(1)	0(1)
O(16)	7(1)	10(1)	9(1)	-1(1)	-2(1)	-2(1)
N(1)	7(1)	10(1)	8(1)	-2(1)	0(1)	-2(1)
N(3)	8(1)	9(1)	9(1)	-2(1)	0(1)	-2(1)

Continued on next page

Table S14 – *Continued from previous page*

	U^{11}	U^{22}	U^{33}	U^{23}	U^{13}	U^{12}
N(2)	7(1)	11(1)	9(1)	-2(1)	0(1)	-2(1)
C(13)	8(1)	12(1)	11(1)	-4(1)	0(1)	-2(1)
C(8)	9(1)	11(1)	9(1)	-4(1)	0(1)	-3(1)
C(12)	7(1)	12(1)	11(1)	-5(1)	0(1)	-3(1)
C(14)	8(1)	11(1)	9(1)	-4(1)	0(1)	-1(1)
C(11)	9(1)	11(1)	11(1)	-4(1)	1(1)	-4(1)
C(15)	9(1)	10(1)	8(1)	-3(1)	0(1)	-1(1)
C(21)	8(1)	10(1)	13(1)	-3(1)	1(1)	-3(1)
C(27)	8(1)	12(1)	10(1)	-3(1)	-1(1)	-3(1)
C(26)	8(1)	13(1)	10(1)	-4(1)	0(1)	-3(1)
C(9)	8(1)	12(1)	11(1)	-4(1)	0(1)	-2(1)
C(10)	8(1)	10(1)	11(1)	-4(1)	0(1)	-2(1)
C(20)	8(1)	10(1)	13(1)	-4(1)	1(1)	-3(1)
C(16)	15(1)	13(1)	10(1)	-2(1)	1(1)	-4(1)
C(25)	13(1)	13(1)	15(1)	-6(1)	1(1)	-3(1)
C(31)	11(1)	14(1)	19(1)	-6(1)	1(1)	-4(1)
C(19)	10(1)	16(1)	12(1)	-6(1)	-1(1)	-2(1)
C(30)	12(1)	18(1)	22(1)	-8(1)	1(1)	-8(1)
C(22)	17(1)	11(1)	15(1)	-2(1)	-1(1)	0(1)
C(24)	17(1)	12(1)	20(1)	-8(1)	2(1)	-1(1)
C(17)	20(1)	15(1)	9(1)	-2(1)	-1(1)	-3(1)
C(28)	8(1)	16(1)	15(1)	-5(1)	-1(1)	-3(1)
C(18)	14(1)	18(1)	10(1)	-4(1)	-4(1)	0(1)
C(23)	18(1)	11(1)	20(1)	-4(1)	-1(1)	2(1)
C(29)	8(1)	20(1)	20(1)	-8(1)	0(1)	-6(1)
C(33)	9(1)	8(1)	10(1)	-1(1)	0(1)	-3(1)
C(32)	8(1)	10(1)	8(1)	-3(1)	1(1)	-2(1)
C(34)	7(1)	11(1)	9(1)	-2(1)	-1(1)	-2(1)
C(45)	9(1)	11(1)	9(1)	-3(1)	0(1)	-2(1)
C(35)	8(1)	10(1)	9(1)	-2(1)	0(1)	-2(1)
C(40)	9(1)	10(1)	9(1)	-2(1)	0(1)	-3(1)
C(37)	10(1)	13(1)	15(1)	-6(1)	0(1)	0(1)
C(39)	8(1)	12(1)	9(1)	-2(1)	0(1)	-2(1)
C(46)	12(1)	17(1)	11(1)	-2(1)	-3(1)	-3(1)

Continued on next page

Table S14 – *Continued from previous page*

	U^{11}	U^{22}	U^{33}	U^{23}	U^{13}	U^{12}
C(41)	12(1)	13(1)	13(1)	-3(1)	1(1)	-6(1)
C(38)	10(1)	12(1)	13(1)	-2(1)	-2(1)	0(1)
C(48)	15(1)	18(1)	11(1)	0(1)	1(1)	-3(1)
C(43)	9(1)	20(1)	13(1)	-3(1)	1(1)	-5(1)
C(49)	10(1)	11(1)	12(1)	0(1)	1(1)	-1(1)
C(44)	8(1)	15(1)	10(1)	-1(1)	0(1)	-2(1)
C(36)	10(1)	13(1)	11(1)	-5(1)	1(1)	-2(1)
C(42)	13(1)	19(1)	15(1)	-5(1)	2(1)	-9(1)
C(47)	18(1)	21(1)	10(1)	-2(1)	-2(1)	-3(1)
C(50)	11(1)	12(1)	8(1)	-3(1)	2(1)	-5(1)
C(56)	9(1)	10(1)	10(1)	-1(1)	-1(1)	-2(1)
N(5)	14(1)	17(1)	11(1)	0(1)	-1(1)	-7(1)
N(4)	12(1)	18(1)	15(1)	-3(1)	3(1)	-6(1)
N(6)	14(1)	14(1)	16(1)	-4(1)	-2(1)	1(1)
C(62)	7(1)	13(1)	12(1)	-4(1)	-1(1)	-2(1)
C(63)	11(1)	16(1)	14(1)	-4(1)	2(1)	-3(1)
C(60)	11(1)	20(1)	19(1)	-2(1)	-4(1)	-4(1)
C(61)	10(1)	20(1)	14(1)	0(1)	0(1)	-5(1)
C(51)	16(1)	12(1)	16(1)	-2(1)	2(1)	-5(1)
C(66)	17(1)	15(1)	22(1)	-6(1)	-4(1)	2(1)
C(64)	16(1)	23(1)	17(1)	-9(1)	5(1)	-3(1)
C(52)	25(1)	15(1)	18(1)	-3(1)	3(1)	-11(1)
C(58)	20(1)	21(1)	11(1)	2(1)	-2(1)	-9(1)
C(59)	18(1)	16(1)	14(1)	0(1)	-5(1)	-5(1)
C(53)	24(1)	24(1)	17(1)	-5(1)	5(1)	-17(1)
C(65)	15(1)	21(1)	24(1)	-12(1)	2(1)	0(1)
C(54)	14(1)	25(1)	18(1)	-6(1)	4(1)	-10(1)
O(17)	20(1)	19(1)	20(1)	-4(1)	1(1)	-3(1)
C(71)	30(1)	26(1)	22(1)	-6(1)	-8(1)	1(1)
C(70)	21(1)	22(1)	24(1)	-6(1)	-1(1)	0(1)
C(69)	24(1)	23(1)	24(1)	-4(1)	5(1)	-8(1)
C(68)	31(1)	22(1)	31(1)	-3(1)	3(1)	-8(1)
N(7)	43(1)	48(1)	45(1)	-25(1)	7(1)	-15(1)
C(72)	55(1)	89(2)	40(1)	-1(1)	6(1)	-36(1)

Continued on next page

Table S14 – *Continued from previous page*

	U^{11}	U^{22}	U^{33}	U^{23}	U^{13}	U^{12}
C(74)	29(1)	55(1)	36(1)	-27(1)	10(1)	-19(1)
F(2)	38(1)	85(1)	50(1)	-47(1)	10(1)	-39(1)
F(3)	47(1)	55(1)	34(1)	-16(1)	9(1)	-37(1)
S(1A)	14(1)	27(1)	13(1)	-10(1)	0(1)	-7(1)
O(6A)	37(1)	73(1)	20(1)	-27(1)	12(1)	-29(1)
O(7A)	21(1)	34(1)	40(1)	-9(1)	-13(1)	2(1)
C(7A)	22(1)	36(1)	36(1)	-23(1)	2(1)	-14(1)
F(1A)	40(1)	25(1)	93(1)	-27(1)	-10(1)	-6(1)
S(1B)	18(2)	18(2)	24(2)	-14(1)	-2(1)	-1(1)
O(6B)	121(19)	80(13)	13(5)	-8(8)	-3(8)	-79(14)
O(7B)	21(1)	34(1)	40(1)	-9(1)	-13(1)	2(1)
C(7B)	22(1)	36(1)	36(1)	-23(1)	2(1)	-14(1)
F(1B)	24(6)	143(16)	46(8)	-18(9)	-12(6)	-7(8)

Bibliography

[1] A. D. Becke *Journal of Chemical Physics*, vol. 98, no. 7, pp. 5648–5652, 1993.

[2] C. T. Lee, W. T. Yang, and R. G. Parr *Physical Review B*, vol. 37, no. 2, pp. 785–789, 1988.

[3] *Jaguar, version 7.6, Schrdinger, LLC, New York, NY, 2011.*

[4] P. J. Hay and W. R. Wadt *Journal of Chemical Physics*, vol. 82, no. 1, pp. 299–310, 1985.

[5] J. M. L. Martin and A. Sundermann *Journal of Chemical Physics*, vol. 114, no. 8, pp. 3408–3420, 2001.

[6] B. Marten, K. Kim, C. Cortis, R. A. Friesner, R. B. Murphy, M. N. Ringnalda, D. Sitkoff, and B. Honig *Journal of Physical Chemistry*, vol. 100, no. 28, pp. 11775–11788, 1996.

[7] Y. Zhao and D. G. Truhlar *Theoretical Chemistry Accounts*, vol. 120, no. 1-3, pp. 215–241, 2008.

[8] T. H. Dunning *Journal of Chemical Physics*, vol. 90, no. 2, pp. 1007–1023, 1989.

[9] M. H. Baik and R. A. Friesner *Journal of physical chemistry A*, vol. 106, pp. 7407–7412, AUG 15 2002.

[10] J. B. Vincent, H. R. Chang, K. Folting, J. C. Huffman, G. Christou, and D. N. Hendrickson *Journal of the American Chemical Society*, vol. 109, no. 19, pp. 5703–5711, 1987.

[11] H. Saltzman and J. G. Sharefkin *Organic Synthesis Collective Volumes*, vol. 5, p. 658, 1973.

[12] P. S. Bryan and J. C. Dabrowiak *Inorganic Chemistry*, vol. 14, no. 2, pp. 296–299, 1975.

[13] E. Y. Tsui, M. W. Day, and T. Agapie *Angewandte Chemie-International Edition*, vol. 50, no. 7, pp. 1668–1672, 2011.

[14] E. Y. Tsui, J. S. Kanady, M. W. Day, and T. Agapie *Chemical Communications*, vol. 47, no. 14, pp. 4189–4191, 2011.

[15] J. S. Kanady, E. Y. Tsui, M. W. Day, and T. Agapie *Science*, vol. 333, no. 6043, pp. 733–736, 2011.

[16] M. W. Wemple, H. L. Tsai, S. Y. Wang, J. P. Claude, W. E. Streib, J. C. Huffman, D. N. Hendrickson, and G. Christou *Inorganic Chemistry*, vol. 35, no. 22, pp. 6437–6449, 1996.

[17] C. C. Stoumpos, I. A. Gass, C. J. Milios, N. Lalioti, A. Terzis, G. Aromi, S. J. Teat, E. K. Brechin, and S. P. Perlepes *Dalton Transactions*, no. 2, pp. 307–317, 2009.

[18] C. C. Stoumpos, T. C. Stamatatos, H. Sartzi, O. Roubeau, A. J. Tasiopoulos, V. Nastopoulos, S. J. Teat, G. Christou, and S. P. Perlepes *Dalton Transactions*, no. 6, pp. 1004–1015, 2009.

[19] P. P. Yang, X. Y. Song, R. N. Liu, L. C. Li, and D. Z. Liao *Dalton Transactions*, vol. 39, no. 27, pp. 6285–6294, 2010.

[20] P. P. Yang and L. C. Li *Inorganica Chimica Acta*, vol. 371, no. 1, pp. 95–99, 2011.

[21] K. Kambe *Journal of the Physical Society of Japan*, vol. 5, no. 1, pp. 48–51, 1950.

[22] *Matlab, 7.10.0.499 (R2010a); The MathWorks, Inc.: Natick, MA, 2010.*

[23] S. Mukherjee, J. A. Stull, J. Yano, T. C. Stamatatos, K. Pringouri, T. A. Stich, K. A. Abboud, R. D. Britt, V. K. Yachandra, and G. Christou *Proceedings of the National Academy of Sciences of the United States of America*, vol. 109, no. 7, pp. 2257–2262, 2012.

[24] R. Tagore, H. Y. Chen, R. H. Crabtree, and G. W. Brudvig *Journal of the American Chemical Society*, vol. 128, no. 29, pp. 9457–9465, 2006.